E. WOLF, PROGRESS IN OPTICS XXVI

V

PHASE-MEASUREMENT INTERFEROMETRY TECHNIQUES

BY

KATHERINE CREATH

WYKO Corporation
1955 East Sixth St., Tucson, AZ 85719, USA

CONTENTS

§ 1. Introduction

High-precision optical systems are generally tested using interferometry, since it often is the only way to achieve the desired measurement precision. To take full advantage of the accuracy available in an interferometric test, interferograms must be analyzed by a computer. The biggest problem is getting the data from an interferogram inside the computer without losing the inherent accuracy contained in the interferogram. In the 1960s, techniques using optical comparators were developed for measuring the position of interference fringe centers, which were sent to a computer for analysis. In the 1970s, faster techniques using graphics tablets or video systems connected to computers were developed for finding fringe centers.

Unfortunately, there are three main problems with these fringe digitization techniques. First, the accuracy of the measured positions of the fringe centers is often less than desired. Generally, an error as large as 1/10 fringe is present in the measurement of a fringe center, whereas the interferometer should have an inherent accuracy of at least an order of magnitude greater than this. Second, not enough data points are obtained in most cases, and data are obtained only at the location of the interference fringes. In order to increase the density of data points, more fringes could be generated by introducing tilt into the interferogram, but then, although more data points are obtained, the accuracy is reduced because of our inability to measure the locations of fringe centers accurately. Third, in most applications it is desirable to analyze fringe data on a uniform square grid. With data obtained only at the location of fringe centers, it is necessary to use some form of interpolation to obtain a square grid of data points from the fringe center data. In addition, the interpolation process can introduce error into the results.

Phase-measurement interferometry (PMI) can be used to overcome these problems. Although the basic techniques for phase-measurement interferometry have been known for several years (CARRÉ [1966], BRUNING, HERRIOTT, GALLAGHER, ROSENFELD, WHITE and BRANGACCIO [1974], SOMMARGREN [1975], WYANT [1975], BRUNING [1978], MASSIE [1980], MOORE and SLAYMAKER [1980], WYANT [1982], WYANT and CREATH [1985]). It is only recently that PMI has become of practical use. Two major developments make

this possible, namely, solid-state detector arrays and fast microprocessors. When a detector array is used to sense fringes, and a known phase change is induced between the object and reference beams, the phase of a wavefront may be directly calculated from recorded intensity data. Generally, a number of data frames are recorded as the reference beam phase is changed in a known manner. The data are shipped to a computer where the phase at each detector point is calculated. Information about the test surface is geometrically related to the calculated wavefront phase.

The direct measurement of phase information has many advantages over simply recording interferograms and then digitizing them. First, the precision of phase-measurement techniques is a factor of ten to a hundred greater than that of digitizing fringes. Second, it is simple. A detector array is placed at the interferogram plane, and a phase-shifting device is placed in the reference beam. Using state-of-the-art solid-state detector arrays, data can be taken very rapidly, thereby reducing errors due to air turbulence or vibration. Third, the data from phase-measurement systems are more precise because the tests can be repeatable to a hundredth or thousandth of a wavelength. By using phase-shifting techniques a contour map of the surface can easily be obtained in a few seconds.

Phase-measurement techniques have been applied to almost all types of interferometer systems. A few interferometer types include Twyman–Green, Mach–Zehnder, Smartt Point-Diffraction, and Mirau and Nomarski interference microscopes. In addition, PMI has also been used with holographic, multiple-wavelength, and speckle interferometer techniques to produce surface countours and deformation measurements (see § 8).

This study describes the basic principles of PMI and ways to implement these techniques into practical interferometric optical testing. Emphasis has been placed on a general treatment of the theory and data processing involved in obtaining a direct measure of a test wavefront relative to a known reference wave. Means of shifting and detecting phase are also discussed. Errors resulting from fundamental limitations, hardware, and software are explained and analyzed. Finally, several applications of PMI are described.

§ 2. Means of Shifting and Determining Phase

There are many ways to determine the phase of a wavefront. For all techniques a temporal phase modulation (or relative phase shift between the object and reference beams in an interferometer) is introduced to perform the

measurement. By measuring the interferogram intensity as the phase is shifted, the phase of the wavefront can be determined with the aid of electronics or a computer.

2.1. MEANS OF PHASE MODULATION

Phase modulation in an interferometer can be induced by moving a mirror, tilting a glass plate, moving a grating, rotating a half-wave plate or analyzer, using an acousto-optic or electro-optic modulator, or using a Zeeman laser (WYANT [1975], SHAGAM and WYANT [1978], WYANT and SHAGAM [1978], HU [1983], KOTHIYAL and DELISLE [1985]). Phase shifters such as moving mirrors, gratings, tilted glass plates, or polarization components can produce continuous as well as discrete phase shifts between the object and reference beams. All of these methods effectively shift the frequency of one beam in the interferometer with respect to the other to introduce a phase difference between beams.

In an interferometer with polarization isolation, the object and reference beams have orthogonal linear or circular polarizations. A rotating half-wave plate (or a quarter-wave plate in double pass) in the output of an interferometer will produce a frequency shift at twice its rotation frequency (see fig. 1A) (SHAGAM and WYANT [1978], WYANT and SHAGAM [1978], HU [1983], KOTHIYAL and DELISLE [1985]). (A rotation of 45° will yield a $\frac{1}{2}\pi$ phase shift.) Likewise, a rotating analyzer will produce a phase modulation at twice the rotation frequency.

Another phase-modulation technique continuously moves a diffraction grating in one arm of the interferometer (fig. 1B). Diffraction gratings produce a wavelength-independent frequency shift in the nth diffracted order of $[nvf]$ when a grating of spatial frequency f is moved with a velocity v (WYANT and SHAGAM [1978]). Instead of a grating, the same effect can be produced using an acousto-optic Bragg cell. In the Bragg cell a traveling acoustic wave serves as a grating, and the frequency shift obtained in the first diffracted order is equal to the device's driving frequency (WYANT and SHAGAM [1978]). A Zeeman laser that has an output of two different frequencies can also produce the phase shift (WYANT and SHAGAM [1978]).

A tilted glass placed in one beam can provide a relative phase shift between object and reference beams (fig. 1C) (WYANT and SHAGAM [1978]). However, this plate must have high optical quality, and care must be taken to have an equal optical path over the entire beam diameter. To minimize aberrations

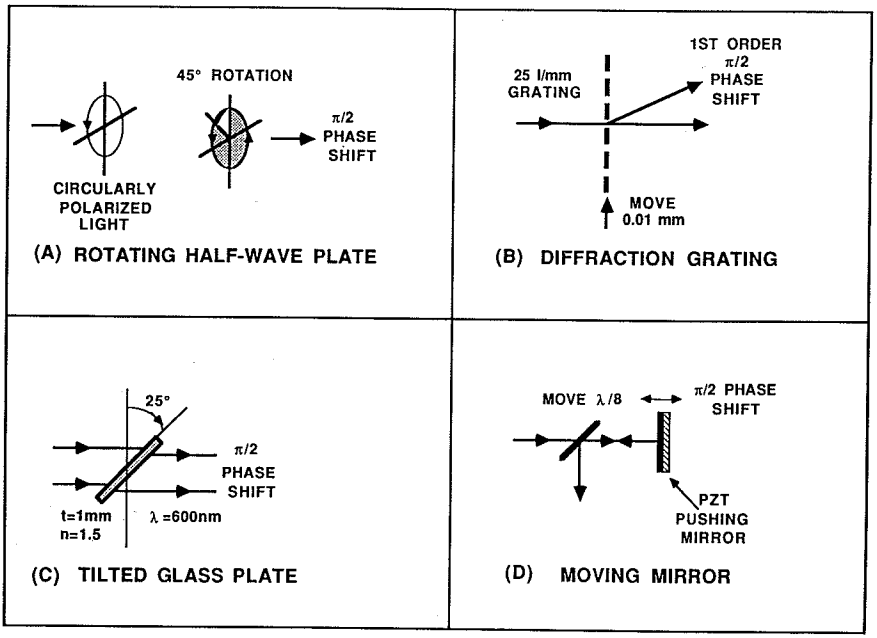

Fig. 1. Means of producing a phase modulation to include (A) a rotating polarizer, (B) a moving diffraction grating, (C) a tilted glass plate, and (D) a moving mirror.

introduced by the plate, it should be placed in a collimated beam. Different amounts of phase shift are achieved by tilting the plate to different angles.

Finally, a common, straightforward phase-shifting technique is the placement of a mirror pushed by a piezo-electric transducer (PZT) in the reference beam (fig. 1D) (WYANT [1982], WYANT and CREATH [1985]). Many brands of PZTs are available to move a mirror linearly over a 1-μm range. A high-voltage amplifier is used to produce a linear ramping signal from 0 to several hundred volts. If there are nonlinearities in the PZT motion, they can be accounted for by using a programmable waveform generator. If a phase-stepping technique is preferred to a continuous modulation, any calibrated PZT can be used because only discrete voltage steps are needed.

2.2.. MEANS OF DETERMINING PHASE

Techniques for determining phase can be split into two basic categories: electronic and analytical. To determine phase electronically, hardware such as

zero-crossing detectors, phase-lock loops, and up-down counters are used to monitor interferogram intensity data as the phase is modulated. For analytical techniques intensity data are recorded while the phase is temporally modulated, sent to a computer, and then used to compute phase. With the advent of powerful desk-top computers and solid-state detector arrays, the analytical techniques have provided the most innovations in this field in the last five years (WYANT and CREATH [1985]). For this reason we will concentrate on the newer techniques and only briefly describe the electronic techniques.

One electronic technique utilizes the detection of a modulated test signal passing through a zero phase value in relation to a modulated reference signal. Zero-crossing techniques measure the time difference between reference and test signals as they pass through a zero (WYANT and SHAGAM [1978]). The wavefront phase is determined to be modulo 2π by taking the ratio between the time measured between crossings and the period of the reference signal. To measure a two-dimensional map of the wavefront, the detector either needs to be scanned or the circuitry must measure the zero crossings at each detector element.

Another technique has been coined phase-lock or ac interferometry (MOORE, MURRAY and NEVES [1978], MOORE and TRUAX [1979], JOHNSON, LEINER and MOORE [1979]). In phase-lock techniques a phase shifter in one interferometer path is modulated sinusoidally with a small amplitude, producing temporally modulated interference terms with cosine of sine and sine of sine dependences. The detected optical signal will contain terms with odd and even order harmonics of the phase modulation frequency. A second, coarser phase-shifter is used to change the path between the two beams in the interferometer until the odd order harmonics (including the fundamental) disappear. When high-order harmonics are filtered out, the resulting electrical signal is directly proportional to the optical phase modulo 2π. With the use of frequency multipliers and up-down counters, phase-lock interferometry can measure phase changes greater than 2π with $\frac{1}{100}\lambda$ repeatabilities. However, to measure over an area, the detector must be scanned.

The last electronic method we will mention has the capability to measure directly a phase change greater than 1 fringe (WYANT and SHAGAM [1978]). Up-down counters enable the actual phase difference to be measured as long as a continuous signal is incident. As a fringe sweeps by the detector, the counter is unchanged, incremented, or decremented depending on its relationship to a known reference signal. Because only changes in phase are measured, the detector must be scanned for area measurements and an uninterrupted signal received. Up-down counters are generally used in conjunction with frequency multipliers in order to measure in units of less than one fringe.

A phase-measurement technique that is analytical but does not use phase-shifting is the Fourier-transform method (TAKEDA, INA and KOBAYASHI [1982], WOMACK [1984a,b]). This method is really a fringe-pattern analysis technique, but we will mention it because it does serve a purpose for systems that are subject to vibration and air turbulence. For this technique a single interferogram is recorded and Fourier transformed. The Fourier spectrum is then bandpass filtered to isolate one of the sidebands. Now the sideband is frequency shifted to be centered at zero frequency. The filtered and shifted spectrum is then inverse Fourier transformed to yield a modulo 2π phase map. This technique does not have as much accuracy as the analytical techniques mentioned in the next section, which directly calculate the phase from a number of phase-shifted interferograms. Because the sidebands are not always isolated, various filters can be used to improve the outcome of these techniques (TAKEDA, INA and KOBAYASHI [1982], WOMACK [1984a,b], KREIS [1986]).

With the developments in solid-state detector arrays, high-speed computers, and computer interfaces, analytical methods enable the phase to be measured as modulo 2π at a number of points in an interferogram simultaneously (WYANT [1982], WYANT and CREATH [1985]). Figure 2 shows a schematic of this type of system with a moving mirror as the phase shifter. There is no need to scan a detector or use a large number of redundant circuits. This type of measurement can have repeatabilities of one-thousandth of a fringe. Other

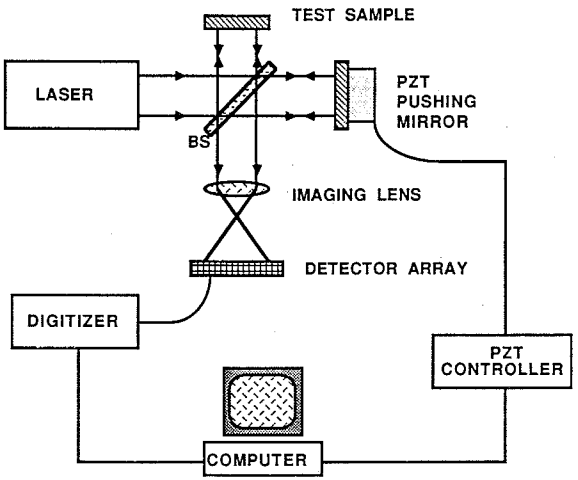

Fig. 2. Twyman–Green interferometer for measuring phase using a PZT pushing a mirror as the phase shifter and sending data to a computer for the phase calculation.

advantages include reduced vibration sensitivity because all the data are taken over the interferogram area in a short period of time, much lower distortion of the interferogram across its area, and the ability to determine noisy or bad data points during the phase calculation.

§ 3. Phase-Measurement Algorithms

Phase-measurement techniques using analytical means to determine phase all have some common denominators. These techniques shift the phase of one beam in the interferometer with respect to the other beam and measure the intensity of an interference pattern at many different relative phase shifts. To make these techniques work, the interference pattern must be sampled correctly to obtain sufficient information to reconstruct the wavefront. The detected intensity modulation as the phase is shifted can be calculated for each detected point to determine if the data point is good. After discussing the sampling requirements, a number of different algorithms for calculating phase are described with equations for the detected intensity modulation. This is followed by a description of the removal of phase ambiguities and the relationship between wavefront phase and the test surface.

3.1. SAMPLING REQUIREMENTS

Fringe modulation is a fundamental problem in all phase-measurement techniques (CREATH [1985]). When a fringe pattern is recorded by a detector array, there is an output of discrete voltages representing the average intensity incident upon the detector element over the integration time. As the relative phase between the object and reference beams is shifted, the intensities read by point detectors should change as shown in fig. 3A. If the interference data are sampled at the Nyquist frequency such that there are two detector elements for each fringe (each half-wave of optical path difference [OPD]), then the wavefront can be reconstructed. However, if the fringe pattern is not sufficiently sampled, the wavefront cannot be correctly reconstructed as shown in fig. 3B, where there is more than one-half fringe per detector. When the area of the detector is finite, the detector reads the average fringe intensity over its area as shown in fig. 3C. As long as there is less than one-half of a fringe per detector element, the intensity will be modulated. However, if there is one fringe over the area of the detector element, there will be no modulation (fig. 3D). Thus,

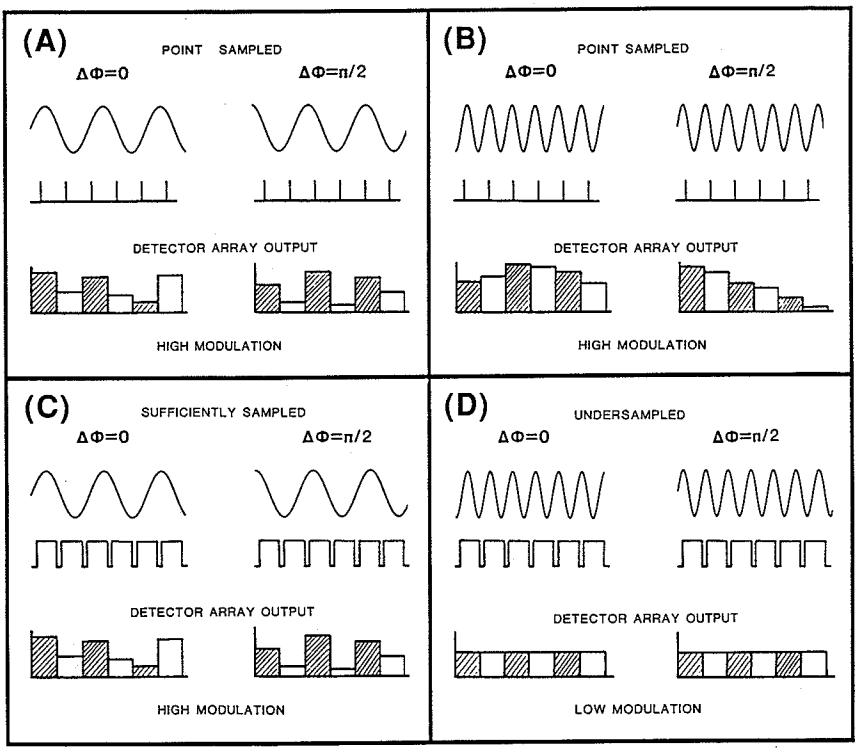

Fig. 3. (A) Sufficient sampling with point detectors showing high modulation of the intensity as the interferometer's relative phase is shifted by $\frac{1}{2}\pi$. (B) Undersampling with point detectors showing aliasing of fringe pattern. (C) Sufficient sampling with finite-sized detectors with $<\frac{1}{2}$ fringe over the detector area. (D) Undersampling with finite-sized detectors showing no intensity modulation.

the detector size influences the recorded fringe modulation, whereas the detector spacing determines if the wavefront can be reconstructed without phase ambiguities.

3.2. GENERAL PHASE-MEASUREMENT TECHNIQUE

Many different algorithms have been published for the determination of wavefront phase (CARRÉ [1966], BRUNING, HERRIOTT, GALLAGHER, ROSENFELD, WHITE and BRANGACCIO [1974], SOMMARGREN [1975], WYANT [1975], BRUNING [1978], SOMMARGREN [1981], MORGAN [1982], WYANT [1982], WYANT, KOLIOPOULOS, BHUSHAN and GEORGE [1984],

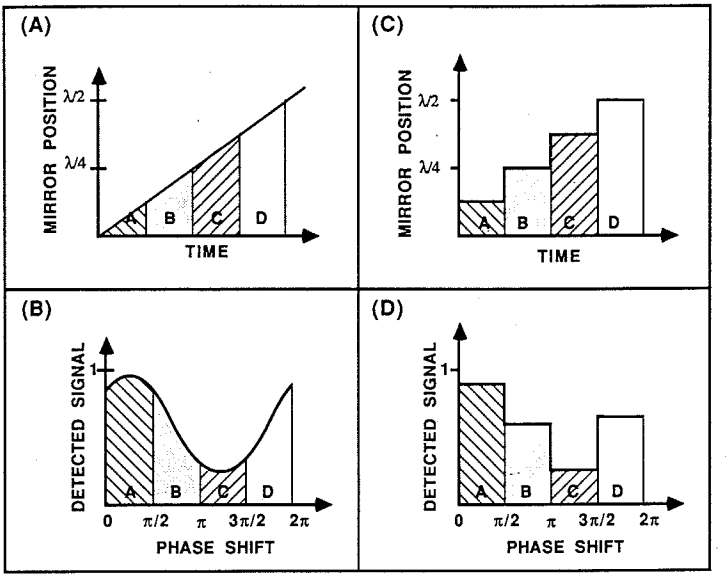

Fig. 4. (A) Mirror position and (B) detected signal for the integrating bucket are shown along with (C) mirror position and (D) detected signal for the phase-stepping technique.

GREIVENKAMP [1984], WYANT and CREATH [1985], REID [1986]). Some techniques step the phase a known amount between intensity measurements, whereas others integrate the intensity while the phase is being shifted. Both types are phase-shifting techniques. The first is usually referred to as a phase-stepping technique, and the second as an integrating-bucket technique. Figure 4 shows the difference between the detected signals in the phase-stepping and integrating-bucket techniques. The number of intensity measurements recorded as the phase is shifted also varies. A minimum of three measurements is necessary to determine the phase, since there are three unknowns in the interference equation

$$I_0 = I_0[1 + \gamma_0 \cos(\phi)] . \tag{3.1}$$

These unknowns are the dc intensity I_0, the modulation of the interference fringes γ_0, and the wavefront phase ϕ. The phase shift between adjacent intensity measurements can be anything between 0 and π as long as it is constant and linear. Since there are so many possible algorithms, we will start a general presentation of the problem and then give specific equations for the most used algorithms.

Normally, N measurements of the intensity are recorded as the phase is shifted. For the general technique the phase shift is assumed to change during the detectors' integration time, and this change is the same from data frame to data frame. The amount of phase change from frame to frame may vary, but it must be known by calibrating the phase shifter or measuring the actual phase change. Unless discrete phase steps are used, the detector array will integrate the fringe intensity data over a change in relative phase of Δ. One set of recorded intensities will be written as (GREIVENKAMP [1984])

$$I_i(x, y) = \frac{1}{\Delta} \int_{\alpha_i - \Delta/2}^{\alpha_i + \Delta/2} I_0(x, y) \{1 + \gamma_0 \cos[\phi(x, y) + \alpha(t)]\} \, d\alpha(t) , \qquad (3.2)$$

where $I_0(x, y)$ is the average intensity at each detector point, γ_0 is the modulation of the fringe pattern, α_i is the average value of the relative phase shift for the ith exposure, and $\phi(x, y)$ is the phase of the wavefront being measured at the point (x, y). The integration over a phase shift Δ makes this expression applicable for any phase-shifting technique. After integrating this expression the recorded intensity is

$$I_i(x, y) = I_0(x, y) \{1 + \gamma_0(\operatorname{sinc} \tfrac{1}{2}\Delta) \cos[\phi(x, y) + \alpha_i]\} , \qquad (3.3)$$

where $\operatorname{sinc} \frac{1}{2}\Delta = (\sin \frac{1}{2}\Delta)/\frac{1}{2}\Delta$. It is important to note that the only difference between integrating the phase and stepping the phase is a reduction in the modulation of the interference fringes after detection. If the phase shift were stepped ($\Delta = 0$) and not integrated, the sinc function would have a value of unity. Therefore, phase stepping is a simplification of the integrating-bucket method. At the other extreme, if $\Delta = 2\pi$, there would be no modulation of the intensity. Since this technique relies on a modulation of the intensities as the phase is shifted, the phase shift per exposure needs to be between 0 and π.

For a total of N recorded intensity measurements the phase can be calculated using a least-squares technique. This type of approach is outlined in detail by both GREIVENKAMP [1984] and MORGAN [1982]. Equation (3.3) is first rewritten in the form

$$I_i(x, y) = a_0(x, y) + a_1(x, y) \cos \alpha_i + a_2(x, y) \sin \alpha_i , \qquad (3.4)$$

where

$$\begin{aligned} a_0(x, y) &= I_0(x, y) , \\ a_1(x, y) &= I_0(x, y) \, \gamma_0(\operatorname{sinc} \tfrac{1}{2}\Delta) \cos \phi(x, y) , \\ a_2(x, y) &= I_0(x, y) \, \gamma_0(\operatorname{sinc} \tfrac{1}{2}\Delta) \sin \phi(x, y) . \end{aligned} \qquad (3.5)$$

The unknowns of this set of equations are $I_0(x, y)$, γ_0 and $\phi(x, y)$, which are represented by $a_0(x, y)$, $a_1(x, y)$, and $a_2(x, y)$. The least-squares solution to these equations is

$$\begin{pmatrix} a_0(x,y) \\ a_1(x,y) \\ a_2(x,y) \end{pmatrix} = \boldsymbol{A}^{-1}(\alpha_i)\, \boldsymbol{B}(x, y, \alpha_i)\,, \tag{3.6}$$

where

$$\boldsymbol{A}(\alpha_i) = \begin{pmatrix} N & \sum \cos\alpha_i & \sum \sin\alpha_i \\ \sum \cos\alpha_i & \sum \cos^2\alpha_i & \sum (\cos\alpha_i)\sin\alpha_i \\ \sum \sin\alpha_i & \sum (\cos\alpha_i)\sin\alpha_i & \sum \sin^2\alpha_i \end{pmatrix}, \tag{3.7}$$

and

$$\boldsymbol{B}(\alpha_i) = \begin{pmatrix} \sum I_i(x,y) \\ \sum I_i(x,y)\cos\alpha_i \\ \sum I_i(x,y)\sin\alpha_i \end{pmatrix}. \tag{3.8}$$

The matrix $\boldsymbol{A}$ needs to be calculated and inverted just once because it is dependent only on the phase shift. The phase at each point in the interferogram is determined by evaluating the value of $\boldsymbol{B}$ at each point and then solving for the coefficients a_1 and a_2:

$$\tan\phi(x,y) = \frac{a_2(x,y)}{a_1(x,y)} = \frac{I_0\gamma_0\,(\operatorname{sinc}\tfrac{1}{2}\Delta)\sin[\phi(x,y)]}{I_0\gamma_0\,(\operatorname{sinc}\tfrac{1}{2}\Delta)\cos[\phi(x,y)]}. \tag{3.9}$$

This phase calculation assumes that the phase shifts between measurements are known and that the integration period Δ is constant for every measurement. Equation (3.9) is sufficient to determine the phase modulo π. To determine the phase modulo 2π, the signs of quantities proportional to $\sin\phi$ and $\cos\phi$ must be examined. This procedure will be discussed in detail at the end of this section.

Besides a reduction in intensity modulation due to the integration over a

change in phase shift, the finite size of the detector element will also contribute to a reduction in intensity modulation, as will extraneous scattered signals incident upon the detector array. To make reliable phase measurements, the incident intensity must modulate sufficiently at each detector point to yield an accurate phase. The recorded intensity modulation can be calculated from the intensity data using the equation

$$\gamma(x, y) = \gamma_0 \operatorname{sinc} \tfrac{1}{2}\Delta = \frac{\sqrt{a_1(x, y)^2 + a_2(x, y)^2}}{a_0(x, y)}. \tag{3.10}$$

This expression can be used to determine if a data point will yield an accurate phase measurement or if it should be ignored. Expressions for the recorded intensity modulation are given for each of the specific techniques described in this section and are used in the examples later in this chapter.

3.3. SYNCHRONOUS DETECTION

An early technique for phase measurement utilized methods of communication theory to perform synchronous detection. To detect a noisy signal synchronously, it is correlated (or multiplied) with sinusoidal and cosinusoidal signals of the same frequency and averaged over many periods of oscillation. The method of synchronous detection as applied by Bruning (BRUNING, HERRIOTT, GALLAGHER, ROSENFELD, WHITE and BRANGACCIO [1974], BRUNING [1978]) to phase measurement can be extracted from the least-squares estimation result when the phase shifts are chosen such that N measurements are equally spaced over one modulation period. With phase shifts α_i such that

$$\alpha_i = \frac{i2\pi}{N}, \quad \text{with} \quad i = 1, \ldots, N,$$

eq. (3.9) reduces to that given by both Bruning and Morgan (BRUNING, HERRIOTT, GALLAGHER, ROSENFELD, WHITE and BRANGACCIO [1974], BRUNING [1978], MORGAN [1982], GREIVENKAMP [1984])

$$\tan \phi(x, y) = \frac{\sum I_i(x, y) \sin(\alpha_i)}{\sum I_i(x, y) \cos(\alpha_i)}. \tag{3.11}$$

For the least-squares estimation of eq. (3.9), eq. (3.11) is the special case in which the matrix A (eq. 3.7) is diagonal.

3.4. FOUR-BUCKET, OR FOUR-STEP, TECHNIQUE

A common algorithm for phase calculations is the four-step, or four-bucket, method (WYANT [1982]). In this case the four recorded sets of intensity measurements can be written as

$$I_1(x, y) = I_0(x, y)\{1 + \gamma \cos[\phi(x, y)]\}, \tag{3.12}$$

$$I_2(x, y) = I_0(x, y)\{1 + \gamma \cos[\phi(x, y) + \tfrac{1}{2}\pi]\} = I_0(x, y)\{1 - \gamma \sin[\phi(x, y)]\}, \tag{3.13}$$

$$I_3(x, y) = I_0(x, y)\{1 + \gamma \cos[\phi(x, y) + \pi]\} = I_0(x, y)\{1 - \gamma \cos[\phi(x, y)]\}, \tag{3.14}$$

$$I_4(x, y) = I_0(x, y)\{1 + \gamma \cos[\phi(x, y) + \tfrac{3}{2}\pi]\} = I_0(x, y)\{1 + \gamma \sin[\phi(x, y)]\}, \tag{3.15}$$

where $\alpha_i = 0, \frac{1}{2}\pi, \pi$ and $\frac{3}{2}\pi$; γ equals γ_0 for the four-step technique and $0.9\gamma_0$ for the four-bucket technique where the phase is integrated over $\Delta = \frac{1}{2}\pi$. Note that integrating the phase produces a very small effect for a $\frac{1}{2}\pi$ phase shift per exposure. Thus, linearly ramping the phase shifter while taking measurements makes more sense than stepping and waiting for the reference beam to settle down. The phase at each point is

$$\phi(x, y) = \tan^{-1}\left(\frac{I_4(x, y) - I_2(x, y)}{I_1(x, y) - I_3(x, y)}\right), \tag{3.16}$$

and the recorded modulation is calculated from

$$\gamma(x, y) = \frac{\sqrt{[I_4(x, y) - I_2(x, y)]^2 + [I_1(x, y) - I_3(x, y)]^2}}{2I_0}. \tag{3.17}$$

3.5. THREE-BUCKET, OR THREE-STEP, TECHNIQUE

Since a minimum of three sets of recorded fringe data is needed to reconstruct a wavefront, the phase can be calculated from a phase shift of $\frac{1}{2}\pi$ (90°) per exposure with $\alpha_i = \frac{1}{4}\pi, \frac{3}{4}\pi$, and $\frac{5}{4}\pi$. The three intensity measurements may be expressed as (WYANT, KOLIOPOULOS, BHUSHAN and GEORGE [1984]).

$$I_1(x, y) = I_0(x, y)\{1 + \gamma \cos[\phi(x, y) + \tfrac{1}{4}\pi]\}, \tag{3.18}$$

$$I_2(x, y) = I_0(x, y)\{1 + \gamma \cos[\phi(x, y) + \tfrac{3}{4}\pi]\}, \tag{3.19}$$

$$I_3(x, y) = I_0(x, y)\{1 + \gamma \cos[\phi(x, y) + \tfrac{5}{4}\pi]\}, \tag{3.20}$$

When discrete steps are used, $\gamma = \gamma_0$, and when the phase is integrated over a $\frac{1}{2}\pi$ phase shift per frame, $\gamma = 0.9\gamma_0$. The phase at each point is then simply

$$\phi(x, y) = \tan^{-1}\left(\frac{I_3(x, y) - I_2(x, y)}{I_1(x, y) - I_2(x, y)}\right), \tag{3.21}$$

and the intensity modulation is

$$\gamma(x, y) = \frac{\sqrt{[I_1(x, y) - I_2(x, y)]^2 + [I_2(x, y) - I_3(x, y)]^2}}{2I_0}. \tag{3.22}$$

If a phase shift of $\frac{2}{3}\pi$ (120°) is used, the three intensity measurements become

$$I_1(x, y) = I_0(x, y)\{1 + \gamma \cos[\phi(x, y) - \tfrac{2}{3}\pi]\}, \tag{3.23}$$

$$I_2(x, y) = I_0(x, y)\{1 + \gamma \cos[\phi(x, y)]\}, \tag{3.24}$$

$$I_3(x, y) = I_0(x, y)\{1 + \gamma \cos[\phi(x, y) + \tfrac{2}{3}\pi]\}, \tag{3.25}$$

where $\gamma = 0.83\gamma_0$ for integration over a $\frac{2}{3}\pi$ phase shift. For these intensity measurements the phase is

$$\phi(x, y) = \tan^{-1}\left(\sqrt{3}\,\frac{I_3(x, y) - I_2(x, y)}{2I_1(x, y) - I_2(x, y) - I_3(x, y)}\right), \tag{3.26}$$

and the detected intensity modulation is

$$\gamma(x, y) = \frac{\sqrt{3[I_3(x, y) - I_2(x, y)]^2 + [2I_1(x, y) - I_2(x, y) - I_3(x, y)]^2}}{2I_0}. \tag{3.27}$$

For a phase shift other than $\frac{1}{2}\pi$ or $\frac{2}{3}\pi$, the phase can be calculated using

$$\phi(x, y) = \tan^{-1}\left(\frac{1 - \cos(\alpha)}{\sin(\alpha)}\,\frac{I_1(x, y) - I_3(x, y)}{2I_2(x, y) - I_1(x, y) - I_3(x, y)}\right), \tag{3.28}$$

where phase shifts of $-\alpha$, 0, and α are assumed. There are many more permutations of these equations, but the foregoing are the most commonly used.

3.6. CARRÉ TECHNIQUE

In the previous equations the phase shift is known either by calibrating the phase shifter or by measuring the amount of phase shift each time it is moved. CARRÉ [1966] presented a technique of phase measurement that is independent of the amount of phase shift. It assumes that the phase is shifted by α between consecutive intensity measurements to yield four equations

$$I_1(x, y) = I_0(x, y)\{1 + \gamma \cos[\phi(x, y) - \tfrac{3}{2}\alpha]\}, \tag{3.29}$$

$$I_2(x, y) = I_0(x, y)\{1 + \gamma \cos[\phi(x, y) - \tfrac{1}{2}\alpha]\}, \tag{3.30}$$

$$I_3(x, y) = I_0(x, y)\{1 + \gamma \cos[\phi(x, y) + \tfrac{1}{2}\alpha]\}, \tag{3.31}$$

$$I_4(x, y) = I_0(x, y)\{1 + \gamma \cos[\phi(x, y) + \tfrac{3}{2}\alpha]\}, \tag{3.32}$$

where the phase shift is assumed to be linear. From these equations the phase shift can be calculated using

$$\tan\tfrac{1}{2}\alpha(x, y) = \sqrt{\frac{3[I_2(x, y) - I_3(x, y)] - [I_1(x, y) - I_4(x, y)]}{[I_2(x, y) - I_3(x, y)] + [I_1(x, y) - I_4(x, y)]}}, \tag{3.33}$$

and the phase at each point is

$$\tan\phi(x, y) = \tan[\tfrac{1}{2}\alpha(x, y)]\frac{[I_2(x, y) - I_3(x, y)] + [I_1(x, y) - I_4(x, y)]}{[I_2(x, y) + I_3(x, y)] - [I_1(x, y) + I_4(x, y)]}. \tag{3.34}$$

To calculate the phase modulo π, the preceding two equations are combined to yield

$$\tan\phi = \frac{\sqrt{[3(I_2 - I_3) - (I_1 - I_4)]\,[(I_2 - I_3) + (I_1 - I_4)]}}{(I_2 + I_3) - (I_1 + I_4)}. \tag{3.35}$$

For this technique the intensity modulation is

$$\gamma = \frac{1}{2I_0}\sqrt{\frac{[(I_2 - I_3) + (I_1 - I_4)]^2 + [(I_2 + I_3) - (I_1 + I_4)]^2}{2}}, \tag{3.36}$$

where this equation assumes that α is near $\frac{1}{2}\pi$. If the phase shift is off by $\pm 10°$, the estimation of γ will be off by $\pm 10\%$. An obvious advantage of the Carré technique is that this phase shift does not need to be calibrated. It also has the advantage of working when a linear phase shift is introduced in a converging or diverging beam where the amount of phase shift varies across the beam.

Equation (3.35) will calculate the phase modulo 2π at each point in the interferogram without worrying about errors resulting from phase calibration difference across the beam.

3.7. REMOVAL OF PHASE AMBIGUITIES

Because of the nature of arctangent calculations, the equations presented for phase calculation are sufficient for only a modulo π calculation. To determine the phase modulo 2π, the signs of quantities proportional to $\sin\phi$ and $\cos\phi$ must be examined. For eq. (3.9) and for all techniques but Carré's, the numerator and denominator give the desired quantities. Table 1 shows how the phase is determined by examining the signs of these quantities after the phase is calculated modulo $\frac{1}{2}\pi$ using absolute values in the numerator and denominator to yield a modulo 2π calculation.

For the Carré technique, simply looking at numerators and denominators is not sufficient to determine phase modulo 2π (CREATH [1985]). In this technique the signs of quantities proportional to $\sin\phi$ and $\cos\phi$ must be examined when using Table 1. One such set of quantities is

$$(I_2 - I_3) = [2I_0\gamma \sin\alpha] \sin\phi . \tag{3.37}$$

$$(I_2 + I_3) - (I_1 + I_4) = [2I_0\gamma \cos\alpha \sin^2\alpha] \cos\phi . \tag{3.38}$$

Figure 5 shows the result of a modulo 2π phase calculation with phase ambiguities that must be removed. Once the phase has been determined to be modulo 2π, the measured wavefront can now be reconstructed using an integration technique that sums up the phases to remove jumps between

TABLE 1
Determination of the phase modulo 2π.

Numerator [$\sin\phi$]	Denominator [$\cos\phi$]	Adjusted phase	Range of phase values
positive	positive	ϕ	0–$\frac{1}{2}\pi$
positive	negative	$\pi - \phi$	$\frac{1}{2}\pi$–π
negative	negative	$\pi + \phi$	π–$\frac{3}{2}\pi$
negative	positive	$2\pi - \phi$	$\frac{3}{2}\pi$–2π
0	anything	π	π
positive	0	$\frac{1}{2}\pi$	$\frac{1}{2}\pi$
negative	0	$\frac{3}{2}\pi$	$\frac{3}{2}\pi$

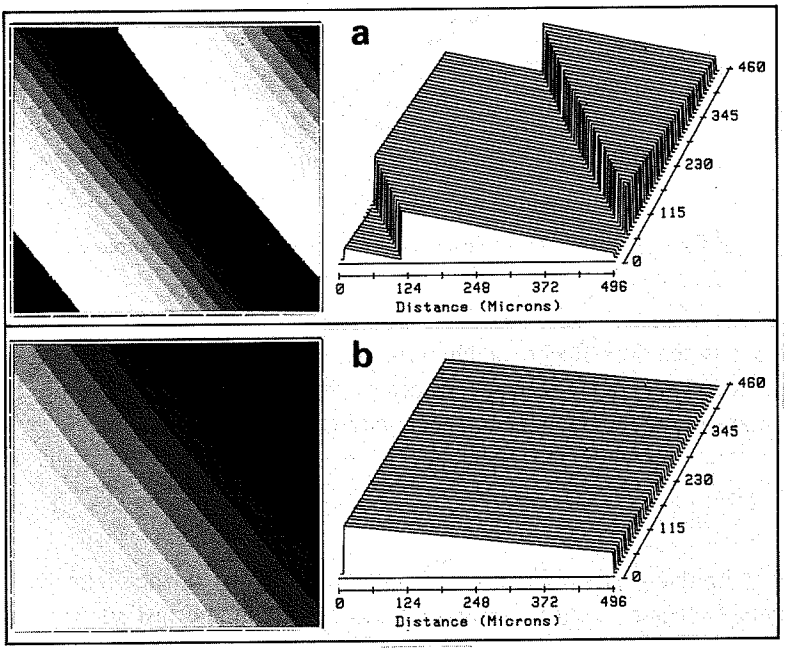

Fig. 5. (A) The results of a modulo 2π calculation and (B) the same data after 2π phase ambiguities have been removed.

adjacent pixels of greater than π. The phase ambiguities due to the modulo 2π calculation can be removed by comparing the phase difference between adjacent pixels. When the phase difference between adjacent pixels is greater than π, a multiple of 2π is added or subtracted to make the difference less than π. For the reliable removal of discontinuities the phase must not change by more than π ($\frac{1}{2}\lambda$ in optical path) between adjacent pixels. As long as the data are sampled as described in the sampling requirements, the wavefront can be reconstructed.

3.8. FROM WAVEFRONT TO SURFACE

Now that the phase of the wavefront is known, the surface shape can be determined from the phase. The surface height H at the location (x, y) is

$$H(x, y) = \frac{\phi(x, y)\,\lambda}{2\pi\,(\cos\theta + \cos\theta')}, \tag{3.39}$$

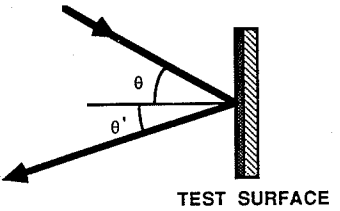

Fig. 6. Definition of the illumination and viewing angles of a surface.

where λ is the wavelength of illumination, and θ and θ' are the angles of illumination and viewing with respect to the surface normal (fig. 6). For a Twyman–Green interferometer this equation is simply

$$H(x, y) = \frac{\lambda}{4\pi} \phi(x, y) . \tag{3.40}$$

This technique yields a direct measurement of the test surface relative to the reference surface. A more accurate measurement of the test surface can be made by measuring the errors due to the interferometer and subtracting them from the results (as shown in § 7). The subtraction eliminates errors caused by aberations in the interferometer or from irregularities in the reference surface.

§ 4. Measurement Example

There are several different equations for calculating the phase of a wavefront from interference fringe intensity measurements. Even though all equations should yield the same result, some algorithms are more sensitive to certain system errors than others (CREATH [1986a]). An example illustrating different results from four different algorithms is shown in this section. A more detailed comparison of these algorithms is given in the section on simulation results. The data for this example were taken using an optical profiler with a flat mirror as the test sample. The mirror was tilted to have two fringes across the diagonal of the field of view. Results are shown for both a calibrated and an uncalibrated system to illustrate the inherent variations between different algorithms. A detector with noticeable nonlinearity was chosen. Figure 7 shows the intensity data taken using a Reticon 256 × 256 detector array with relative phase shifts of 90° between consecutive data frames. Five frames are shown where the first and the last frames should have a 360° phase shift between them. This shows

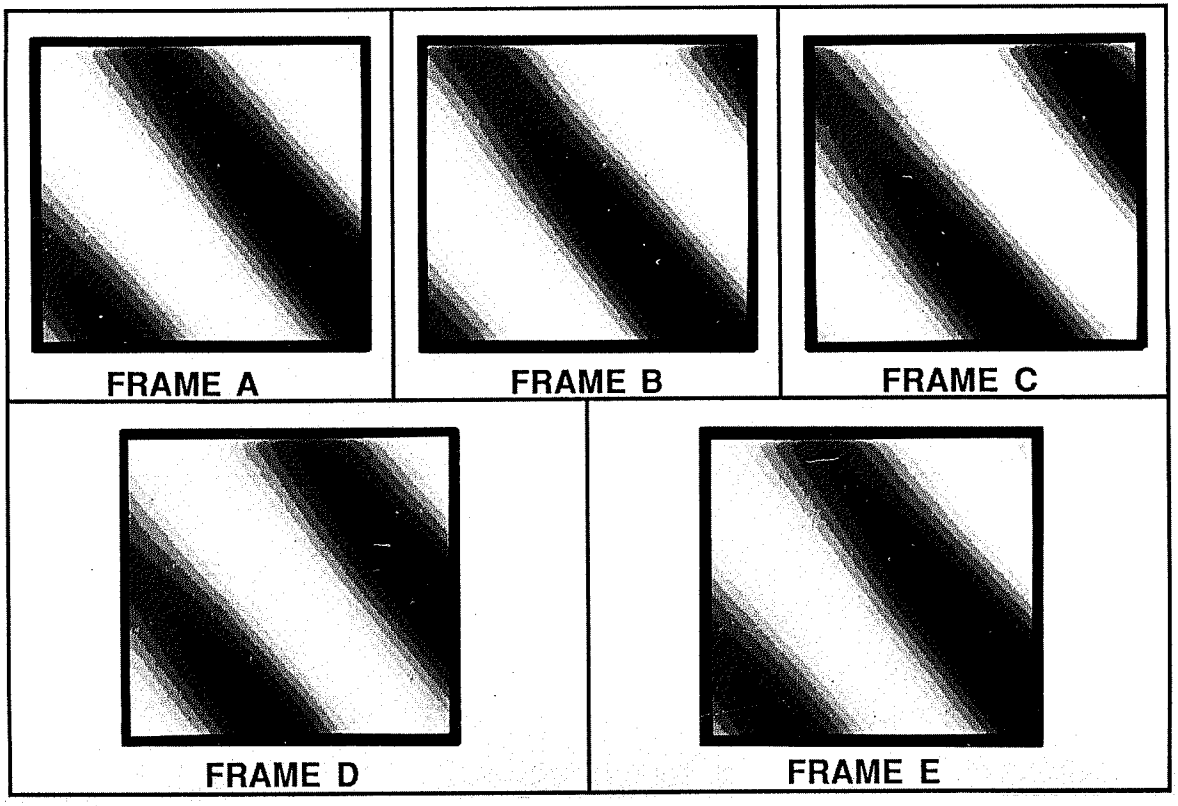

Fig. 7. Five frames of fringe intensity data with 90° phase shifts between adjacent frames. For a calibrated system the first and fifth frames will overlap. Page 369: gray-level plots; page 370: contour plots.

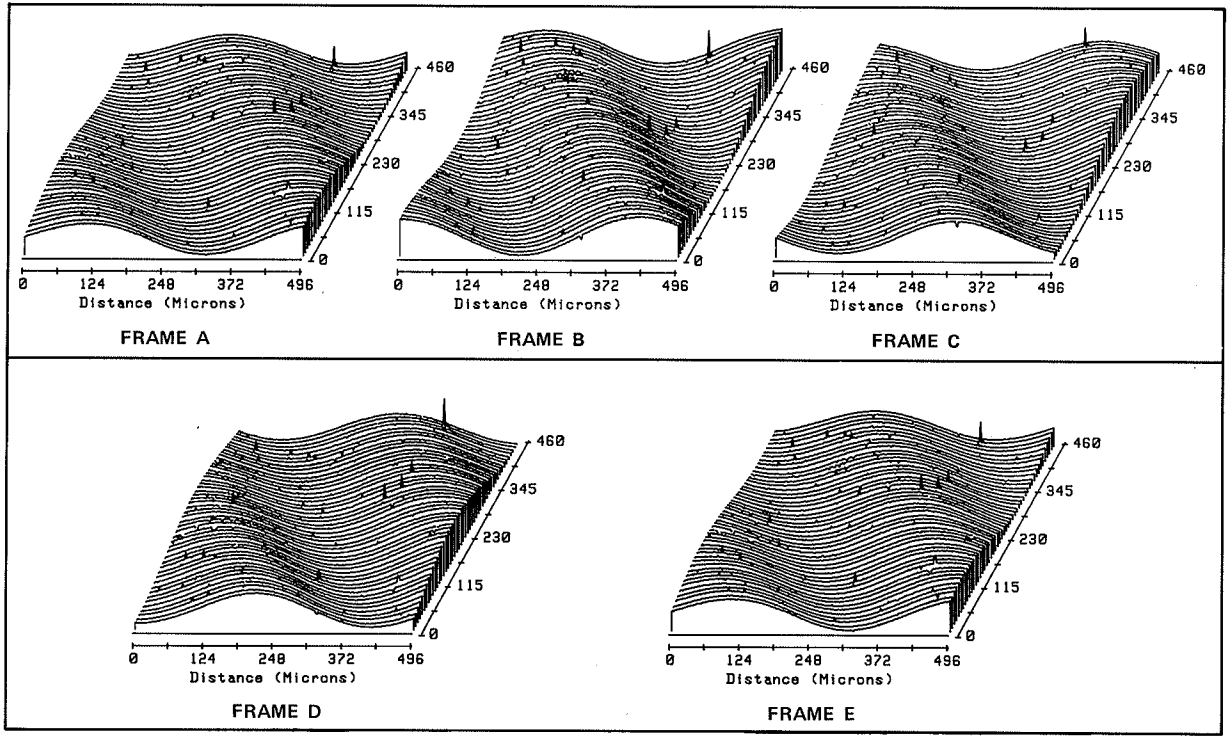
460
345
230
115
0
0 124 248 372 496
Distance (Microns)
FRAME A
FRAME B
FRAME C
FRAME D
FRAME E

Fig. 7. (cont'd).

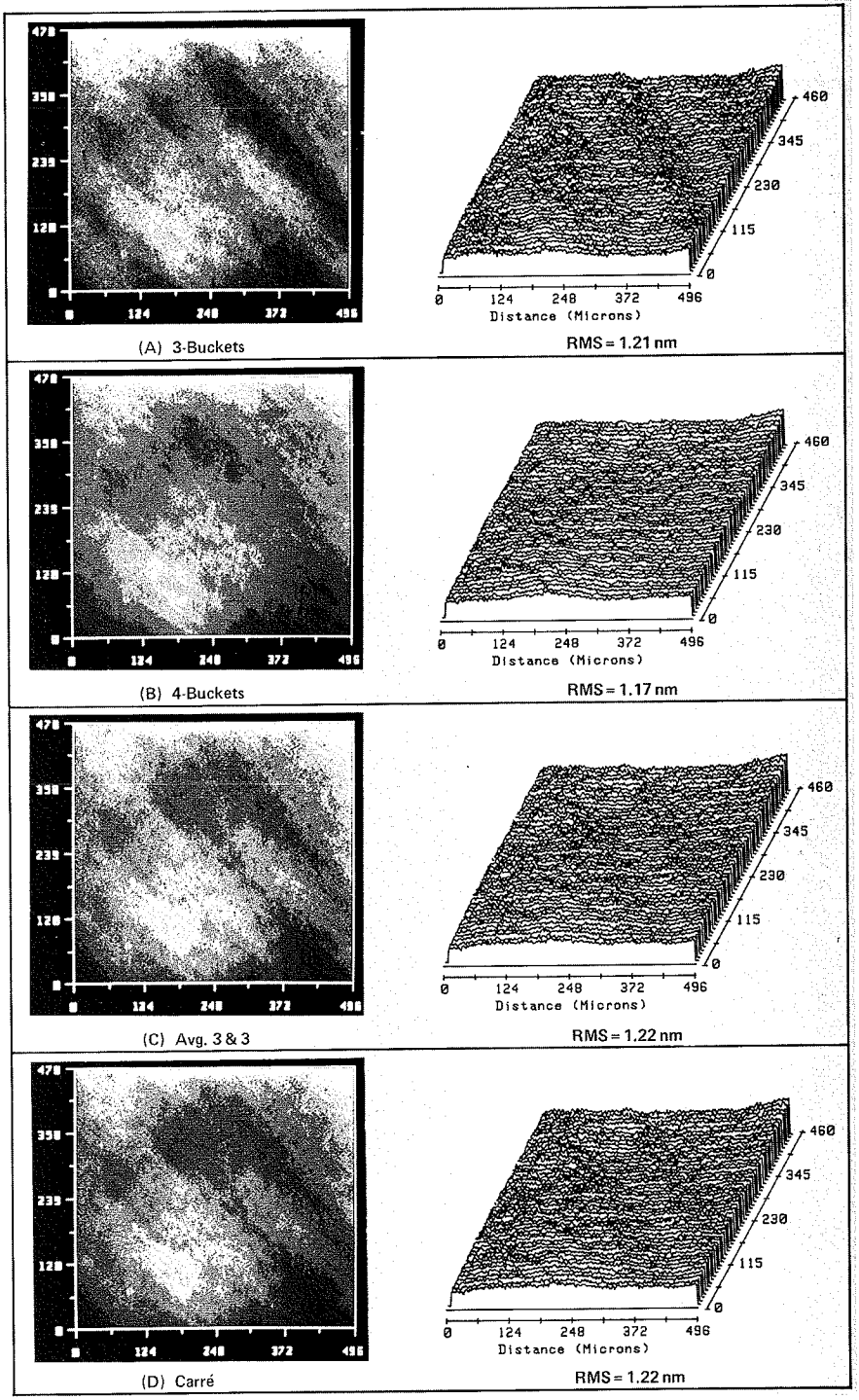

Fig. 8. Results of calculating phase using four different algorithms with the same fringe intensity data containing two fringes across a flat mirror. The interferometer is calibrated for 90° of phase shift between data frames. All plots in figs. 8, 9, and 12 are on the same height scale.

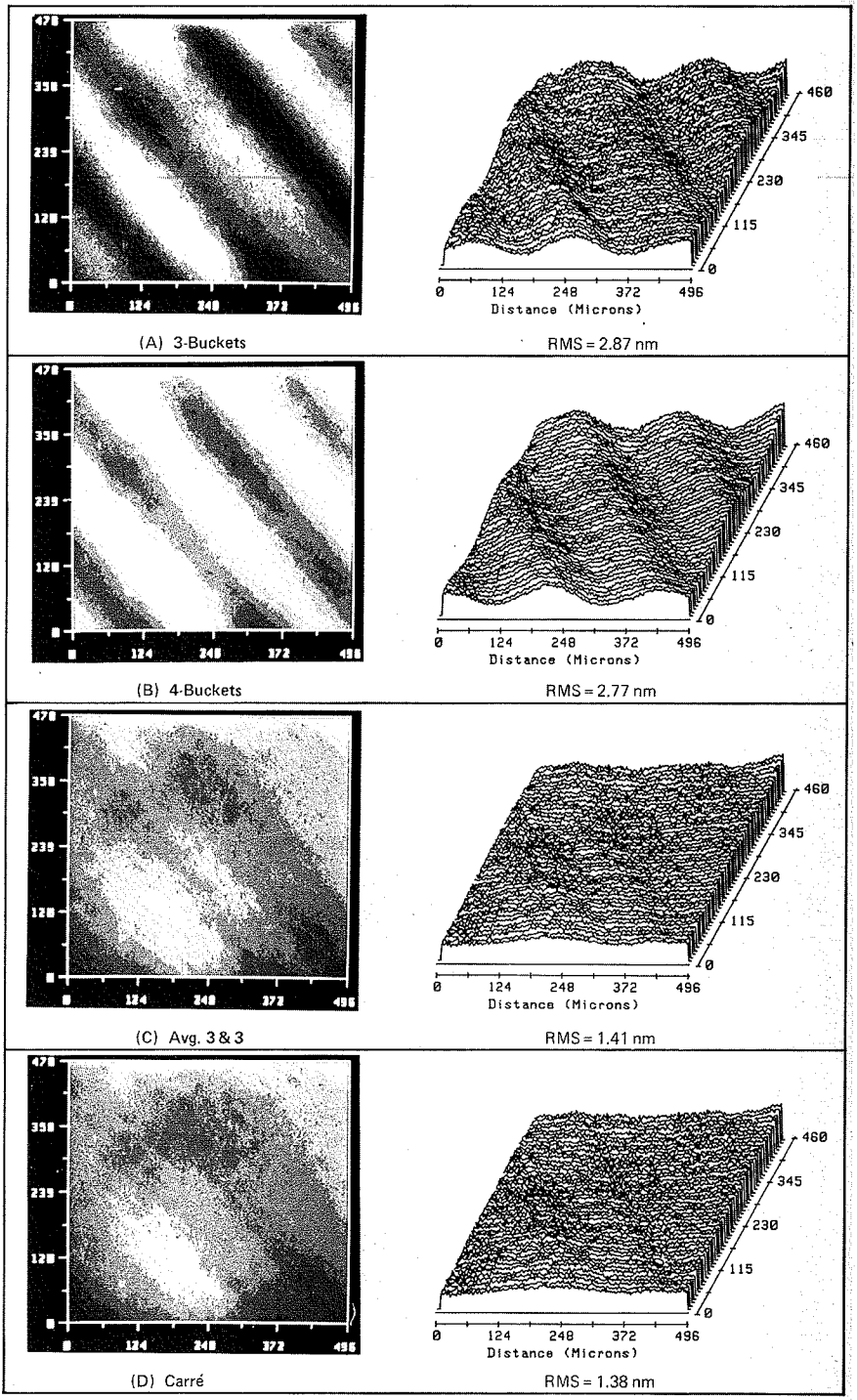

Fig. 9. Results of calculating phase using four different algorithms with the same fringe intensity data containing two fringes across a flat mirror. The interferometer is miscalibrated for 82° of phase shift between data frames.

that the phase shifter is indeed calibrated, since frame A and frame E overlap very well. The spikes in the intensity data are due to either bad pixels in the array or dust and defects on the sample. The results of calculating the phase using four different equations with the same four sets of intensity data are shown in fig. 8. Similar calculations for a miscalibration of the phase shifter are shown in fig. 9 after new data were taken at the same location on the surface with a relative phase shift of 82°. Some of the results for the miscalibrated phase shifter show an error with a sinusoidal dependence, whereas other do not. When the phase shifter is calibrated (fig. 8), much of the sinusoidal error goes away, but there is still some waviness noticeable in the calculated phases. The behavior of these errors will be examined in the next section.

§ 5. Error Analysis

The precision of a phase-measuring interferometer system can be determined by taking two measurements, subtracting them, and looking at the root-mean-square of the difference wavefront. For a well-calibrated system this result should be less than $\frac{1}{100}\lambda$. However, this method does not tell us much about the actual accuracy of the measurement. Accuracy is normally determined relative to some standard. The measurement accuracy will be degraded by system errors such as miscalibration of the phase shifter, nonlinearities due to the detector, quantization of the detector signal, the reference surface, aberrations in the optics of the interferometer, air turbulence, and vibrations. Air turbulence and vibrations are dynamic variables that contribute to both the system measurement precision and the accuracy. By placing the interferometer on a vibration-isolated table, enclosing the beam paths, and taking data fast, the effects of vibration and air turbulence can be minimized. In order to achieve a $\frac{1}{100}\lambda$ measurement, the detector signal should be digitized to at least 8 bits, and the interferometer intensity should be adjusted to cover the full range of the detector. Errors caused by miscalibration of the phase shifter can be eliminated by careful calibration of the system. Errors caused by an inaccurate reference surface or aberrations in the interferometer optics can be subtracted out by the methods outlined in § 7. However, some errors such as a nonlinear phase shifter or a nonlinear detector will limit the ultimate accuracy of the measurement. These errors are discussed in more detail in the following section. The choice of phase-measurement algorithm can reduce one error at the expense of others. A simulation comparing the behavior of different algorithms for phase-shifter and detector errors is shown in § 6.

5.1. PHASE-SHIFTER ERRORS

Phase errors caused by inaccurate phase-shifter calibration can be minimized by adjusting the interferometer for a single fringe. However, with large amounts of aberration present, it may not be possible to obtain a single fringe. If a constant calibration error is present, the phase shift may be written as

$$\alpha' = \alpha(1 + \varepsilon), \tag{5.1}$$

where α is the desired phase shift, α' is the actual phase shift, and ε is the normalized error. For phase stepping it has been shown that the errors in phase resulting from a calibration error or nonlinearity in the phase shifter will decrease as the number of measurements increases (SCHWIDER, BUROW, ELSSNER, GRZANNA, SPOLACZYK and MERKEL [1983]). The same should be true for integrating-bucket techniques. For a consistent phase-shift error, such as a miscalibration, a periodic error is seen in the calculated phase, which has a spatial frequency of twice the fringe spacing (see fig. 9). Nonlinear phase-shift errors are not as easy to deal with or detect. A quadratic nonlinear phase-shift error can be written as

$$\alpha' = \alpha(1 + \varepsilon\alpha). \tag{5.2}$$

In normal operation a nonlinear phase shifter will be partially compensated in the calibration of the interferometer by adding a linear bias to its movement. The most straightforward approach to calibration is to make sure that the phase shifter actually moves 2π over a 2π desired change in phase. This error term can be realized by adding a normalized linear compensation term of an equal and opposite amplitude to eq. (5.2). The phase shift is then replaced with

$$\alpha' = \alpha(1 + \varepsilon\alpha - \varepsilon). \tag{5.3}$$

This function minimizes the error caused by nonlinear phase-shifter motion. Nonlinear phase-shifter errors can be reduced by applying certain algorithms such as the Carré technique and the averaging-three-and-three technique described later; however, they cannot be eliminated.

5.2. PHASE-SHIFTER CALIBRATION

The value of the phase shift α can be determined in a number of ways. A good indication of α can be obtained by taking four frames of intensity data and using eq. (3.33) to calculate the phase shift at each detector point. The phase-shift

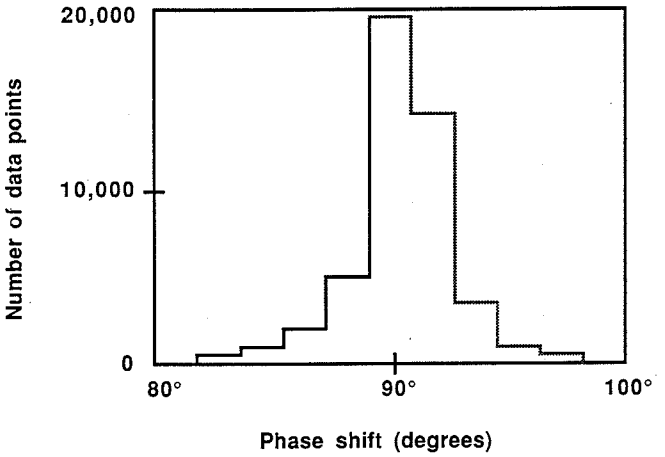

Fig. 10. Histogram showing the distribution of phase shifts for a well-calibrated phase shifter. The distribution should be a narrow Gaussian centered around the desired phase shift.

controller should be adjusted so that the average phase shift is at the desired value and the spread in calculated phase shifts is small (see fig. 10). A simpler equation can be used when five intensity measurements are taken with the same phase shift α between them (SCHWEIDER, BUROW, ELSSNER, GRZANNA, SPOLACZYK and MERKEL [1983], CHENG and WYANT [1985a]). The phase shift is then calculated from

$$\alpha(x, y) = \cos^{-1}\left[\frac{1}{2}\left(\frac{I_5(x, y) - I_1(x, y)}{I_4(x, y) - I_2(x, y)}\right)\right]. \tag{5.4}$$

Another technique to determine phase shift involves extracting linear slices across a set of fringes for each of the phase shifts. These slices are then differentiated and the fringe peaks and valleys are found by interpolation to determine the amount of phase shift. A more visual means of adjusting the phase shift is to plot these linear sections of fringes for $N + 1$ intensity measurements with shifts in increments of $2\pi/N$. The $(N + 1)$th measurement should overlap the first measurement (see fig. 11).

Alternatively, the actual phase shift can be determined over the shifter's range by observing a reference signal that indicates the phase difference between the two interferometer beams. The reference signal can be generated by splitting off some of the light from the reference arm of the interferometer and directing it into a small interferometer and separate detector (HAYES [1984]). When a

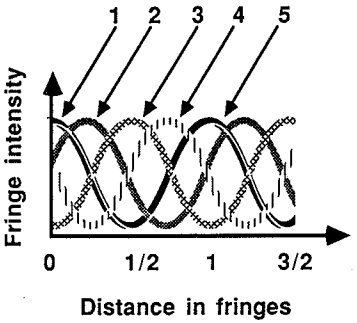

Fig. 11. Calibration of the phase shifter by overlapping linear traces of the interference fringes for the first and $(N + 1)$th data frames.

computer controls the phase shifter, the driving voltage for the device is usually stored as an array, which is read out each time the shifter is employed. A sinusoidal intensity modulation can be obtained by linearly changing the phase of the reference beam. However, the signal that provides a linear phase shift will not necessarily be linear because of shifter nonlinearities. The signal that provides a linear phase shift can be determined by using a reference detector (HAYES [1984]) and measuring the actual phase shift obtained, and then calculating the proper shifter motion, or by doing a least-squares fit (AI and WYANT [1987]).

If a phase-stepping technique is being used, the actual phase shift can be determined by the computer and reference detector each time the phase shift is changed. With this information each phase step can be corrected to use algorithms requiring equal phase shifts, or the actual phase shift for each data frame can be plugged into the least-squares calculation of eq. (3.6).

5.3. AVERAGING-THREE-AND-THREE TECHNIQUE

SCHWIDER, BUROW, ELSSNER, GRZANNA, SPOLACZYK and MERKEL [1983] proposed a technique of reducing errors that averages two phase measurements taken with a relative phase shift of $\frac{1}{2}\pi$ between the two measurements. One realization of this technique involves taking four measurements as in the four-bucket technique, calculating the phase using eq. (3.21) for the first three buckets, and averaging this with the phase calculated using eq. (3.21) with the last three of the four buckets. This procedure can be expressed mathemati-

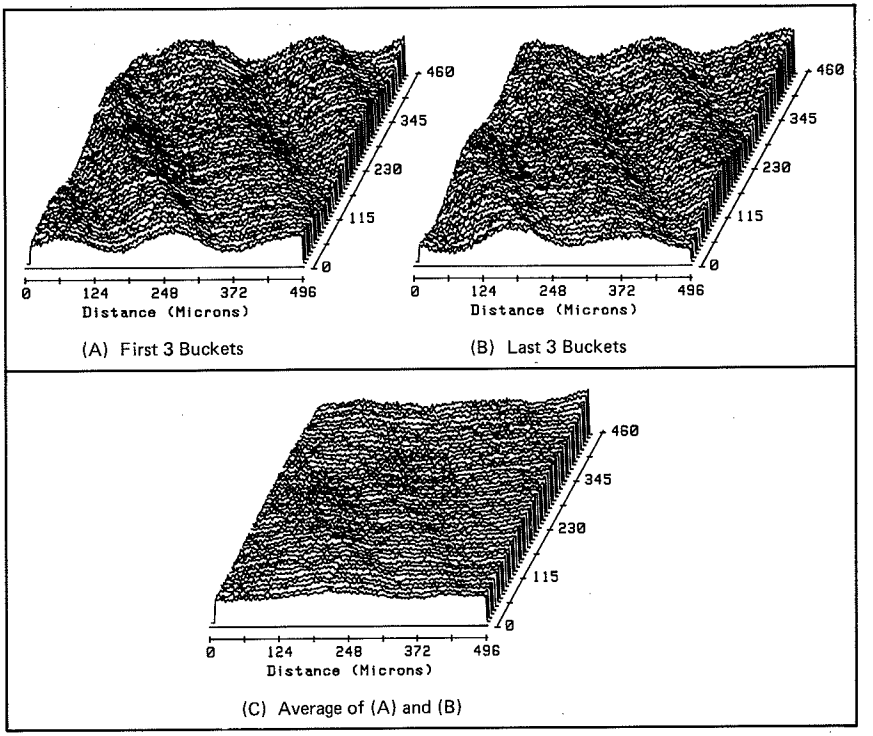

Fig. 12. Example showing the improvement realized by averaging the phase calculated using the first three of four buckets with the phase calculated using the last three of four buckets.

cally as

$$\phi(x,y) = \tfrac{1}{2}\left[\tan^{-1}\left(\frac{I_3(x,y) - I_2(x,y)}{I_1(x,y) - I_2(x,y)}\right) + \tan^{-1}\left(\frac{I_4(x,y) - I_3(x,y)}{I_2(x,y) - I_3(x,y)}\right)\right]. \tag{5.5}$$

This tevchnique has the advantage of being simple to calculate and yet has the ability to average out errors. Figure 12 shows sample data where the phase from the first three buckets is shown to have sinusoidal errors caused by a phase-shift miscalibration that is directly out of phase with the phase calculated from the last three buckets. When the phases from the first three and last three buckets are averaged, the sinusoidal error term is significantly reduced.

5.4. DETECTOR NONLINEARITIES

A nonlinear response from a detector can introduce phase errors, which are especially noticeable if they are not consistent from detector to detector in an array. Many CCD-type detector arrays read out the odd and even rows through different shift registers. If the gains in the two sets of registers are not equal and nonlinear, bothersome errors arise that must be removed.

When a detector has a second-order nonlinear response, the measured optical irradiance I' can be written in terms of the incident optical irradiance I as

$$I' = I + \varepsilon I^2 , \tag{5.6}$$

where ε is the nonlinear coefficient. Expanding the detected irradiance of the fringe pattern, the interference equation (3.1) becomes

$$I' = I_0[1 + \gamma\cos(\phi + \alpha) + \varepsilon I_0^2[1 + 2\gamma\cos(\phi + \alpha) + \gamma^2\cos^2(\phi + \alpha)] , \tag{5.7}$$

$$I' = I_0[1 + \varepsilon I_0] + I_0[1 + 2\varepsilon I_0]\gamma\cos(\phi + \alpha) + \varepsilon I_0^2\gamma^2\cos^2(\phi + \alpha)] , \tag{5.8}$$

$$I' = I_0' + I_0''\gamma\cos(\phi + \alpha) + \tfrac{1}{2}\varepsilon[I_0\gamma]^2\{1 + \cos[2(\phi + \alpha)]\} , \tag{5.9}$$

where α indicates the phase shift for a particular exposure. The nonlinearity in eq. (5.9) will cause phase errors. When eq. (5.9) is substituted into the four-bucket calculation of eq. (3.16), the 2ϕ dependent terms will cancel in the numerator and denominator. Once the third terms cancel, the coefficients of the other terms in eq. (5.9) only reduce the measured fringe modulation and will not affect the measurement. If, however, eq. (5.9) were substituted into the three-bucket calculation of eq. (3.21), the nonlinearities add and cause large

TABLE 2
Harmonics due to detection nonlinearities.

Number of buckets	Harmonic order									
	2	3	4	5	6	7	8	9	10	11
3	2	–	4	5	–	7	8	–	10	11
4	–	3	–	5	–	7	–	9	–	11
5	–	–	4	–	6	–	–	9	–	11

phase errors. Thus, when a second-order nonlinearity is present in the detected irradiance, a minimum of four measurements is necessary to obtain an accurate phase calculation. For higher-order nonlinearities, STETSON and BROHINSKY [1985] have determined which orders of detection errors will affect the measurement for small numbers of phase steps. The dashes in Table 2 indicate which detection nonlinearity orders do not contribute to phase errors in the various algorithms. In most cases the largest distortions affecting the measurement are probably due to third-order harmonics,

$$I' = I + \varepsilon I^3 , \tag{5.10}$$

so that five steps should be enough to reduce most effects of detector nonlinearities.

§ 6. Simulation Results

The experimental results shown earlier indicate that the results of PMI calculations depend on the algorithm used. The most desirable algorithm depends on the particular PMI system. In general, the more intensity measurements, the less error there will be in the calculated phase values. This section endeavors to find the best algorithm using the fewest number of measurements for systems that are susceptible to phase-shifter and detector errors. The techniques compared in these simulations are: (1) three-bucket technique of eq. (3.21); (2) four-bucket technique of eq. (3.16); (3) Carré technique of eq. (3.35); (4) averaging-three-and-three technique of eq. (5.5); and (5) a five-bucket technique using the synchronous detection outlined in eq. (3.11).

The simulated error terms are plotted in fig. 13 for particular values of ε in eqs. (5.1), (5.3), (5.6) and (5.10). Because the errors in the phase calculations are not symmetrical, both positive and negative errors are shown. The actual phase shifts with errors are plotted versus the desired degrees of phase shift. Note that the linear compensation error for the nonlinear error shifts the actual phase by 360° when 360° is desired, but intermediate values are wrong. In the integrating bucket techniques the phase shift is continuously moved along these values, but for phase-stepping techniques there are discrete values at the desired phase shifts. The detection nonlinearities show plots of the detector output signal versus the incident intensity, assuming a perfect detector behaves linearly.

The simulations are performed by starting with a known phase function, which varies from 0° to 360° over 1000 data points. The fringe intensity

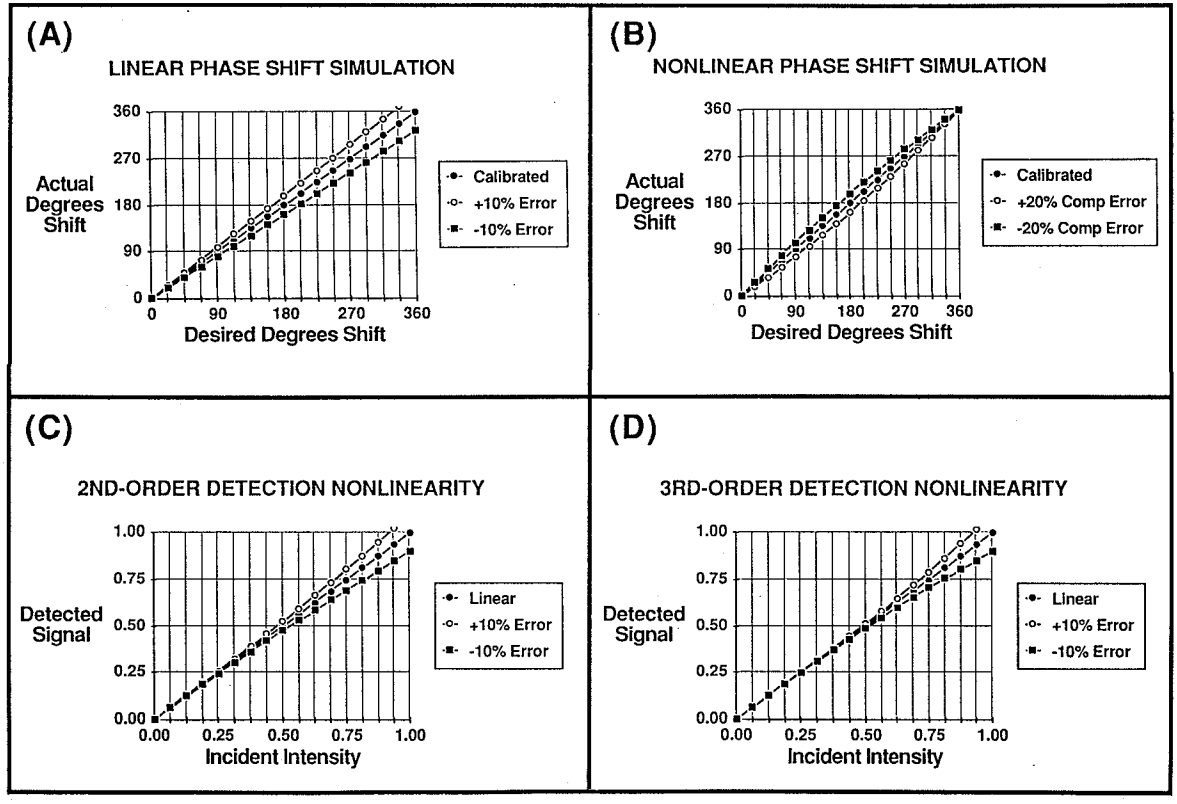

Fig. 13. Plots of error functions used in the computer-calculated error simulations.

measurements for the different techniques are then calculated using the appropriate equations by both the integrating-bucket technique and the phase-stepping technique with an equivalent fringe modulation. If a phase-shift error is present, it is applied when the fringe intensities are calculated. Detection errors are added after the intensities have been calculated. Once the intensity data are fabricated, the phase is calculated from these data. The error in the calculation is the difference between the calculated phases and the original phase function. These simulations are performed for the five phase-measurement algorithms at 21 different error values ranging from -20% to $+20\%$.

Phase-shift errors in waves (number of wavelengths) are shown in fig. 14 for

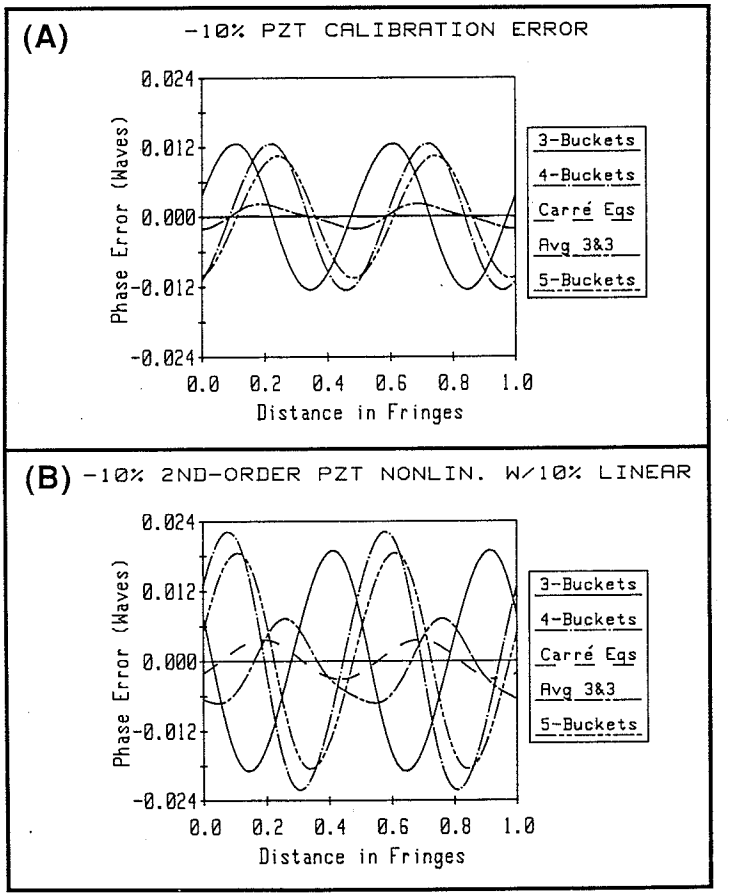

Fig. 14. Results for simulation of phase-shifter errors with (A) -10% linear error and (B) -10% second-order error, compensated by $+10\%$ linear error.

a simulated wavefront containing one fringe of tilt in optical path difference across the wavefront. All five techniques show a quasi-sinusoidal dependence in the error terms for both miscalibration and a nonlinear phase shifter. The frequency of the sinusoid is twice that of the input fringe intensity data. Figure 15 shows the calculated peak-to-valley (P–V) phase-shifter errors in waves plotted versus percent simulated error. The Carré technique shows no errors for the linear phase-shift error because it is tailored for this situation. A miscalibration error can be reduced substantially by the averaging-three-and-three technique (see fig. 12). With nonlinear phase-shifter errors present, the

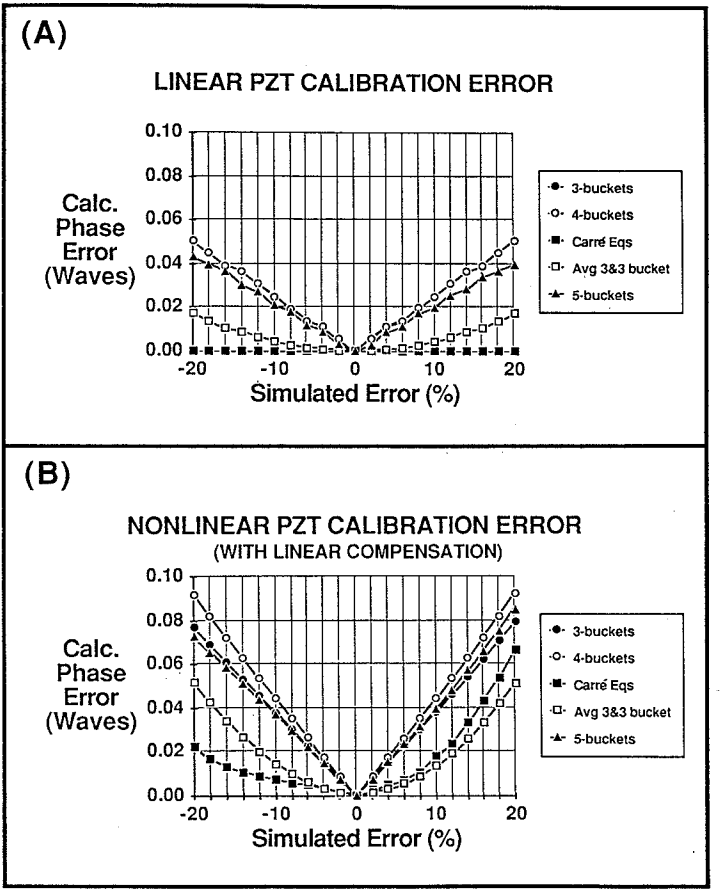

Fig. 15. Simulation results of phase-shifter errors for all five algorithms with error amounts ranging from −20% to +20%.

Carré equations reduce the error to give a slightly better result than averaging-three-and-three; however, they do not completely eliminate it. For all phase-shifter errors the three-bucket and four-bucket techniques show the most error. Even though these techniques yield the largest error, the magnitude of that error is less than $\frac{1}{20}$ of a wave for a 10% error in the phase shift. The errors from the detection nonlinearities are shown versus one fringe in optical path in fig. 16. These results show a more complicated frequency structure than the phase-shift errors. The frequency of the errors is four times the fringe frequency. Figure 17 shows plots of the second- and third-order detection nonlinear errors

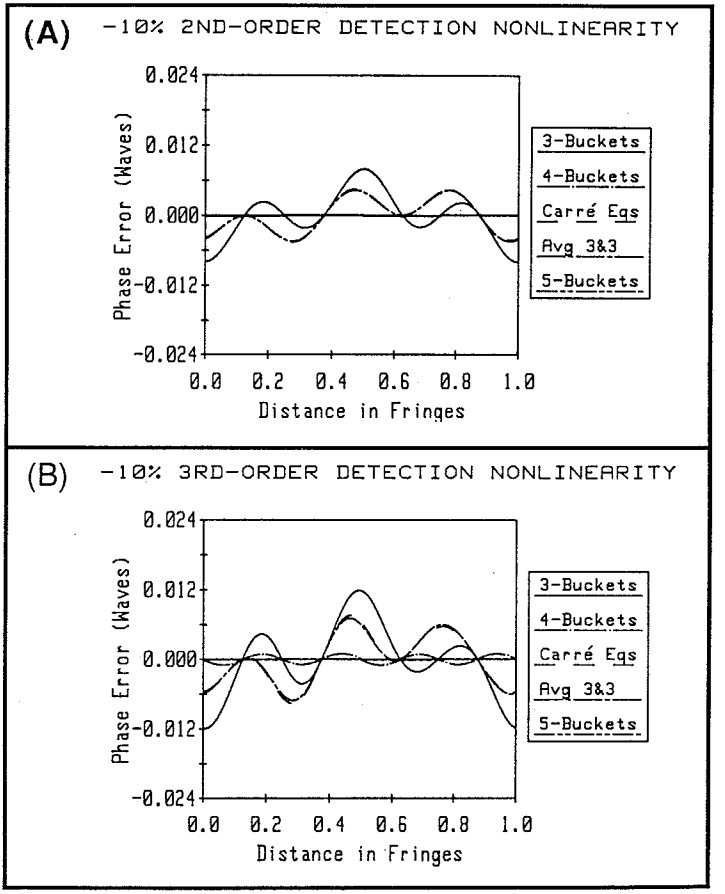

Fig. 16. Results for simulation of detection errors with (A) −10% second-order error and (B) −10% third-order error.

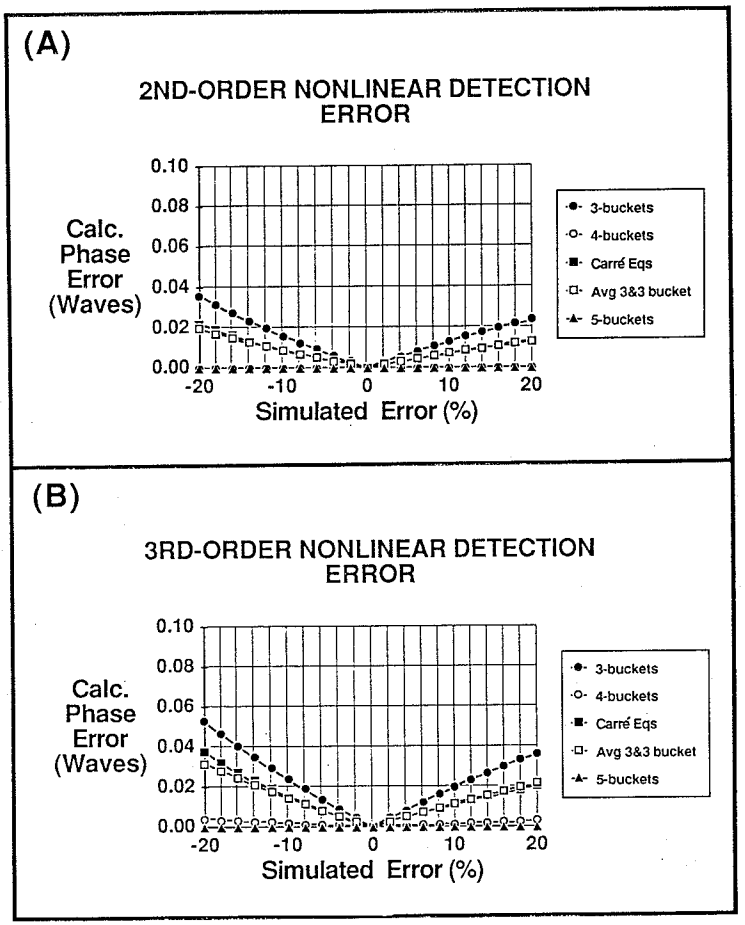

Fig. 17. Simulation results of nonlinear detection errors for all five algorithms with error amounts ranging from -20% to $+20\%$.

versus the percentage of simulated error. Note that these have been plotted on the same scale as the phase-shift errors. As shown in the last section, the four-bucket and five-bucket techniques are insensitive to second-order detection nonlinearities, and the five-bucket technique is insensitive to third-order nonlinearities, whereas the four-bucket technique shows very little sensitivity to the third-order nonlinearity. The three-bucket technique again shows the greatest sensitivity to the simulated errors. For both second and third orders the averaging-three-and-three technique and the Carré technique have similar

amounts of error, which are a factor of two better than the three-bucket technique, but not nearly as good as the four- and five-bucket techniques.

Looking back at the experimental results in § 4 (figs. 8 and 9), which had two fringes of tilt in the field view, it is obvious that the Carré technique behaves the best for a miscalibration and that the three- and four-bucket techniques are the worst. When the system phase shifter is calibrated, there still is a waviness in the results most likely caused by a detection nonlinearity. Because the four-bucket results are best, most of the error is probably due to a detection nonlinearity.

This simulation study has shown that certain phase-measurement algorithms yield better results in the presence of some system errors than others. It also shows that the P–V magnitude of these errors is well within $\frac{1}{10}$ of a wave even with a 20% error. In general, the integrating-bucket methods give the same results as the phase-stepping methods except in the case of nonlinear phase-shift errors, where the integrating-bucket method is superior. The Carré algorithm is the best to use for phase-shifting errors, and the four- and five-bucket techniques are best for eliminating effects due to second- and third-order detection nonlinearities. If speed of calculation is a factor, the averaging-three-and-three technique, which averages errors, can give passable results in all cases. This study also found that the more buckets used, the less error due to the system is seen in the result.

§ 7. Removing System Aberrations

Errors that reduce the measurement accuracy can be caused by reference surface errors or aberrations present in the interferometer. The elimination of these errors depends on the type of measurement being performed. In all cases a measurement of system errors can be made using a very good mirror as the test object. When the test mirror is of better quality than the optics contained in the interferometer, the wavefront measured from this surface will represent the aberrations in the interferometer. This aberrated wavefront can then be subtracted from subsequent measurements using the test objects. The reference wavefront must be measured again whenever the focus, tilt, or zoom of an interferometer is changed, because these factors change the amount of aberration.

If random high-frequency errors are present, and a very good surface is not available, a more involved technique is needed, for which many phase measurements of the flat must be averaged (WYANT [1985]). In between measurements

the test surface is moved by a distance greater than the correlation length of irregularities on the surface. This ensures statistically independent measurements. With the averaging of statistically independent portions of the test surface, the test surface errors are reduced by the square root of the number of measurements. The errors in the interferometer are then the major contributors to the averaged wavefront. Once the reference wavefront is obtained, it is subtracted from subsequent tests to improve accuracy. If only the root-mean-square (rms) of the test surface is desired, two measurements are needed (WYANT [1985]). First, the surface is measured, and then the test surface is moved a distance greater than the correlation length and measured again. The rms of the difference in the phases for the two measurements yields $\sqrt{2}$ times the rms of the test surface independent of any errors in the reference surface.

The preceding technique works well for surface roughness measurement, but when surface figure is measured, a different approach is necessary. Absolute calibration of any curved surface can be performed using three measurements (JENSEN [1973], BRUNING [1978]). The test surface is first measured to yield the wavefront phase $W_{0°}$, then rotated 180° and measured again to obtain $W_{180°}$. A third measurement W_{focus} is taken by translating the test surface until the apex of the test surface is at the focal point of the diverger (or converger) lens. The three measurements can be summed up as follows:

$$W_{0°} = W_{\text{surf}} + W_{\text{ref}} + W_{\text{div}}, \tag{7.1}$$

$$W_{180°} = \overline{W}_{\text{surf}} + W_{\text{ref}} + W_{\text{div}}, \tag{7.2}$$

$$W_{\text{focus}} = W_{\text{ref}} + \tfrac{1}{2}(W_{\text{div}} + \overline{W}_{\text{div}}), \tag{7.3}$$

where "surf" indicates the surface we are trying to measure, "ref" refers to errors due to system aberrations in the reference arm, "div" refers to errors in the test arm and the diverger lens, and the overscores indicate a 180° rotation of that wavefront contribution. When all three wavefronts have been calculated, the wavefront resulting from the surface under test is given by

$$W_{\text{surf}} = \tfrac{1}{2}[W_{0°} + \overline{W}_{180°} - W_{\text{focus}} - \overline{W}_{\text{focus}}). \tag{7.4}$$

Likewise, the aberrations in the interferometer including the reference surface and the diverger lens can be calculated using

$$W_{\text{aber}} = W_{\text{ref}} + W_{\text{div}} = \tfrac{1}{2}(W_{0°} - \overline{W}_{180°} + W_{\text{focus}} + \overline{W}_{\text{focus}}). \tag{7.5}$$

Once the system aberrations are measured, this wavefront (W_{aber}) can be subtracted from subsequent measurements to provide an accurate measure of the test surface as long as the reference surface, diverging optics, and imaging

optics are not moved. Flats can also be measured absolutely by comparing three surfaces (SCHULZ and SCHWIDER [1976], FRITZ [1984]).

An example using eq. (7.5) to create a reference to subtract from test measurements is shown in fig. 18. Figure 18A shows a measurement taken

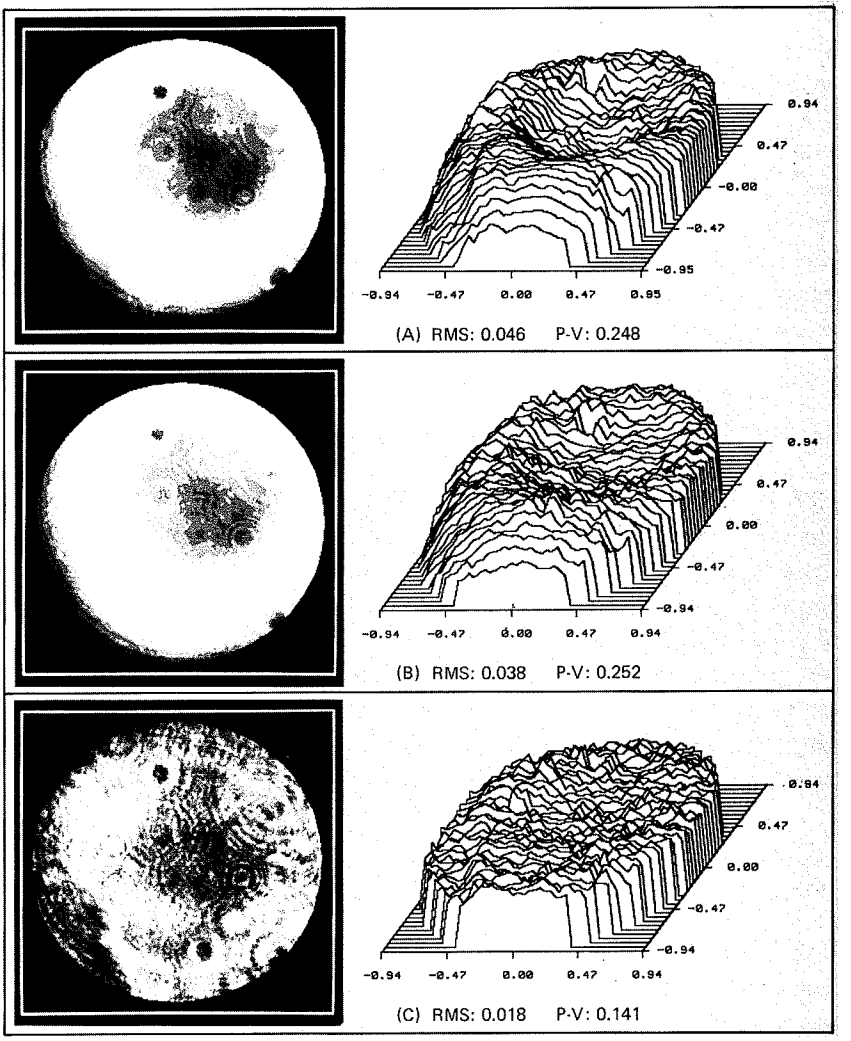

Fig. 18. PMI results of measuring (A) a spherical mirror using a 20× microscope objective as the diverger lens, (B) the reference wavefront created using the technique of eq. (7.5), and (C) the measurement of the mirror minus the reference wavefront, which yields an absolute measurement of the spherical mirror.

using a Twyman–Green interferometer with a PZT pushing the reference mirror as the phase shifter. Tilt and focus have been subtracted from all the wavefronts in the figure. A standard 20× microscope objective was used to generate a spherical wave to test an F/2 mirror, which was good to $\frac{1}{50}\lambda$ over the F/8 measurement area. Because the microscope objective was used at incorrect conjugates, a lot of spherical aberration in the measurement limited the accuracy of the measurement. A reference wavefront was generated using the technique of eq. (7.5) to produce a wavefront containing the aberrations in the interferometer and the microscope objective (fig. 18B). When this reference is subtracted from the measurement of fig. 18A, the result (fig. 18C) is independent of the interferometer accuracy. The results show a mirror with an rms surface quality of $\frac{1}{50}\lambda$. Under normal circumstances better diverging optics would be used to test a spherical mirror; however, the best results will be obtained when a reference wavefront containing interferometer errors is subtracted from the test wavefront.

§ 8. Applications of Phase-Measurement Interferometry

Phase-measurement interferometry (PMI) can be applied to any two-beam interferometer, including holographic interferometers. Applications can be divided into three major types of measurement: surface figure, surface roughness, and metrology. The measurement of surface figure finds the shape of a test surface (usually an optical surface) relative to a reference mirror. Surface roughness measurements are interested in the surface microstructure and its statistics rather than the shape of the piece. Metrology is used to find out properties of a sample such as the homogeneity of an optical material or the deformation of a surface.

8.1. SURFACE SHAPE MEASUREMENT

The traditional measurements in interferometry have been to measure the shape of an optical component such as a lens or mirror. Surface figure measurements can also include desensitized tests such as using computer-generated holograms, two-wavelength holography, or two-wavelength phase-shifting interferometry to measure surfaces with large departures from the reference surface. The desensitized tests either use a reference surface close to the shape of the test surface created by a null lens or a computer-generated

hologram, or they synthesize a longer wavelength using interferograms from different wavelength measurements (two-wavelength holography and two-wavelength phase-shifting interferometry) or by projecting fringes onto the object surface (digital moiré). Surface figure measurements are used to test both smooth surfaces such as optical flats, spheres, and aspheres, and rough surfaces of machined parts with arbitrary shapes.

Recent techniques for measuring surface figures are the use of a radial shear or lateral shear interferometer to measure aspheric surfaces (HARIHARAN, OREB and ZHOU WANZHI [1984], YATAGAI and KANOU [1983, 1984]). Since the measurement is proportional to the slope of the surface under test, the sensitivity can be varied by changing the amount of shear. Another shearing interferometer using PMI techniques utilizes a Ronchi grating to produce the shear (YATAGAI [1984]). For aspheric surfaces a useful technique based on two-wavelength holography (WYANT, OREB and HARIHARAN [1984]) for measuring surface shape is two-wavelength phase-shifting interferometry (CHENG and WYANT [1984, 1985b], FERCHER, HU and VRY [1985], CREATH, CHENG and WYANT [1985], CREATH and WYANT [1986], CREATH [1986b]). In this technique the phases measured at two different wavelengths are subtracted and then 2π ambiguities are removed. This test synthesizes a wavefront as if it were measured at an equivalent wavelength $\lambda_{eq} = \lambda_1\lambda_2/|\lambda_1 - \lambda_2|$. The test sensitivity is varied by changing wavelengths.

For measurements where the interferometer system is subject to vibration or air turbulence, many techniques have been developed to obtain all the information in a very short period of time. One method uses a grating to code the information on a single detector array (MCLAUGHLIN [1986]). Another method uses a grating in a Smartt point-diffraction interferometer to produce four phase-shifted interferograms on four different detectors simultaneously (KWON [1984]). Still other techniques produce the phase-shifted interferograms in different ways (SMYTHE and MOORE [1984]).

For measurements of very irregular surfaces PMI has been applied to both holographic interferometry techniques (WYANT, OREB and HARIHARAN [1984], HARIHARAN and OREB [1984], THALMANN and DÄNDLIKER [1984, 1985a]), and moiré techniques (YATAGAI, IDESAWA, YAMASHI and SUZUKI [1982], WOMACK [1984a,b], BELL and KOLIOPOULOS [1984]). In holographic techniques a hologram of the object is illuminated using either a different wavelength of illumination or by changing the angle of the reference beam. In moiré techniques, fringes are projected on the object and viewed (with or without a reference grating) as the projected fringes are phase shifted using a detector array.

8.2. SURFACE ROUGHNESS MEASUREMENT

To measure the microstructure of a surface, an interference microscope is used to resolve 1-μm surface areas laterally with height resolutions in the ångstrom range. These instruments use the same phase-measurement techniques as the surface figure measurements. But rather than measuring a smooth, continuous surface figure, these instruments measure profiles of random-looking surfaces. Optical profilers have been used to test super-smooth optical surfaces as well as magnetic tape, floppy disks, and magnetic read/write heads.

Optical profilers using PMI techniques have been based on different types of interference microscopes. Some have been based on the Nomarski type of microscope, which splits the illumination into two polarizations and compares one to the other, giving a measure of the surface slope (SOMMARGREN [1981], EASTMAN and ZAVISLAN [1983], ZAVISLAN and EASTMAN [1985], JABR [1985]). Others utilize objectives that compare the surface to a reference surface with a Mirau, Michelson, or Linnik interferometric objective (WYANT, KOLIOPOULOS, BHUSHAN and GEORGE [1984], BHUSHAN, WYANT and KOLIOPOULOS [1985], WYANT, KOLIOPOULUS, BHUSHAN and BASILA [1985]). Still other optical profilers look more like standard interferometers than microscopes (MATTHEWS, HAMILTON and SHEPPARD [1986], SASAKI and OKAZAKI [1986], PANTZER, POLITCH and EK [1986]).

8.3. METROLOGY

The use of PMI techniques in optical metrology is relatively new. In addition to measuring beam profiles (HAYES and LANGE [1983]) and the homogeneity or index profile of an optical material (MOORE and RYAN [1978, 1982]), these techniques enable the measurement of sample properties by determining the deformation of an object caused by temperature changes, pressure changes, stress, or strain, as well as studying the vibration properties of mechanical components.

Holographic interferometry has traditionally been used to measure object deformations and vibrations, but only qualitative information was available. PMI has been applied to all types of holographic interferometric measurement, from looking at deformations (SOMMARGREN [1977], HARIHARAN, OREB and BROWN [1982, 1983a,b], DÄNDLIKER and THALMANN [1985], HARIHARAN [1985], KREIS [1986]) to measuring the amplitude and phase of an object

vibration (OSHIDA, IWATA and NAGATA [1983], NAKADATE [1986b], HARIHARAN and OREB [1986]). Recently, PMI measurements have also been applied to speckle interferometry techniques, which are similar to holographic interferometry techniques but do not require the making of an intermediate hologram (WILLEMIN and DÄNDLIKER [1983], NAKADATE and SAITO [1985], STETSON and BROHINSKY [1985], CREATH [1986c], ROBINSON and WILLIAMS [1986], NAKADATE [1986a]).

8.4. FUTURE POSSIBILITIES

Future developments in phase-measurement interferometry will most likely be continuations of these applications to more irregular surfaces. Larger detector arrays will enable the measurement of steeper surfaces and allow holographic applications without the need to produce an intermediate hologram. Likewise, faster computers and parallel processing will allow us to view wavefront measurements in real time.

References

AI, C., and J.C. WYANT, 1987, Appl. Opt. **26**, 1112.

BELL, B.W., and C.L. KOLIOPOULOS, 1984, Opt. Lett. **9**, 171.

BHUSHAN, B., J.C. WYANT and C.L. KOLIOPOULOS, 1985, Appl. Opt. **24**, 1489.

BRUNING, J.H., 1978, Fringe scanning interferometers, in: Optical Shop Testing, ed. D. Malacara (Wiley, New York).

BRUNING, J.H., D.R. HERRIOTT, J.E. GALLAGHER, D.P. ROSENFELD, A.D. WHITE and D.J. BRANGACCIO, 1974, Appl. Opt. **13**, 2693.

CARRÉ, P., 1966, Metrologia **2**, 13.

CHENG, Y.-Y., and J.C. WYANT, 1984, Appl. Opt. **23**, 4539.

CHENG, Y.-Y., and J.C. WYANT, 1985a, Appl. Opt. **24**, 3049.

CHENG, Y.-Y., and J.C. WYANT, 1985b, Appl. Opt. **24**, 804.

CREATH, K., 1985, Appl. Opt. **24**, 3053.

CREATH, K., 1986a, Proc. SPIE **680**, 19.

CREATH, K., 1986b, Proc. SPIE **661**, 296.

CREATH, K., 1986c, Direct measurements of deformations using digital speckle-pattern interferometry, in: Proc. SEM Spring Conf. on Experimental Mechanics, New Orleans (Society for Experimental Mechanics, Bethel, CT) p. 370.

CREATH, K., and J.C. WYANT, 1986, Proc. SPIE **645**, 101.

CREATH, K., Y.-Y. CHENG and J.C. WYANT, 1985, Opt. Acta **32**, 1455.

DÄNDLIKER, R., and R. THALMANN, 1985, Opt. Eng. **24**, 824.

EASTMAN, J.M., and J.M. ZAVISLAN, 1983, Proc. SPIE **429**, 56.

FERCHER, A.F., H.Z. HU and U. VRY, 1985, Appl. Opt. **24**, 2181.

FRITZ, B.S., 1984, Opt. Eng. **23**, 379.
GREIVENKAMP, J.E., 1984, Opt. Eng. **23**, 350.
HARIHARAN, P., 1985, Opt. Eng. **24**, 632.
HARIHARAN, P., and B.F. OREB, 1984, Opt. Commun. **51**, 142.
HARIHARAN, P., and B.F. OREB, 1986, Opt. Commun. **59**, 83.
HARIHARAN, P., B.F. OREB and N. BROWN, 1982, Opt. Commun. **41**, 393.
HARIHARAN, P., B.F. OREB and N. BROWN, 1983a, Appl. Opt. **22**, 876.
HARIHARAN, P., B.F. OREB and N. BROWN, 1983b, Proc. SPIE **370**, 189.
HARIHARAN, P., B.F. OREB and ZHOU WANZHI, 1984, Opt. Acta **31**, 989.
HAYES, J., and S. LANGE, 1983, Proc. SPIE **429**, 22.
HAYES, J.B., 1984, Linear Methods of Computer Controlled Optical Figuring, Ph.D. Dissertation (Optical Sciences Center, University of Arizona, Tucson, AZ).
HU, H.Z., 1983, Appl. Opt. **22**, 2052.
JABR, S.N., 1985, Opt. Lett. **10**, 526.
JENSEN, A.E., 1973, J. Opt. Soc. Am. **63**, 1313.
JOHNSON, G.W., D.C. LEINER and D.T. MOORE, 1979, Opt. Eng. **18**, 46.
KOTHIYAL, M.P., and C. DELISLE, 1985, Appl. Opt. **24**, 2288.
KREIS, T., 1986, J. Opt. Soc. Am. A **3**, 847.
KWON, O.Y., 1984, Opt. Lett. **9**, 59.
MASSIE, N.A., 1980, Appl. Opt. **19**, 154.
MATTHEWS, H.J., D.K. HAMILTON and C.J.R. SHEPPARD, 1986, Appl. Opt. **25**, 2372.
MCLAUGHLIN, J., 1986, Proc. SPIE **680**, 35.
MOORE, D.T., and D.P. RYAN, 1978, J. Opt. Soc. Am. **68**, 1157.
MOORE, D.T., and D.P. RYAN, 1982, Appl. Opt. **21**, 1042.
MOORE, D.T., and B.E. TRUAX, 1979, Appl. Opt. **18**, 91.
MOORE, D.T., R. MURRAY and F.B. NEVES, 1978, Appl. Opt. **17**, 3959.
MOORE, R.C., and F.H. SLAYMAKER, 1980, Appl. Opt. **19**, 2196.
MORGAN, C.J., 1982, Opt. Lett. **7**, 368.
NAKADATE, S., 1986a, Appl. Opt. **25**, 4155.
NAKADATE, S., 1986b, Appl. Opt. **25**, 4162.
NAKADATE, S., and H. SAITO, 1985, Appl. Opt. **24**, 2172.
OSHIDA, Y., K. IWATA and R. NAGATA, 1983, Opt. Lasers Eng. **4**, 67.
PANTZER, D., J. POLITCH and L. EK, 1986, Appl. Opt. **25**, 4168.
REID, G.T., 1986, Opt. Lasers Eng. **7**, 37.
ROBINSON, D.W., and D.C. WILLIAMS, 1986, Opt. Commun. **57**, 26.
SASAKI, O., and H. OKAZAKI, 1986, Appl. Opt. **25**, 3137.
SCHULZ, G., and J. SCHWIDER, 1976, Interferometric testing of smooth surfaces, in: Progress in Optics, Vol. XIII, ed. E. Wolf (North-Holland, Amsterdam) pp. 93.
SCHWIDER, J.R., R. BUROW, K.-E. ELSSNER, J. GRZANNA, R. SPOLACZYK and K. MERKEL, 1983, Appl. Opt. **22**, 3421.
SHAGAM, R.N., and J.C. WYANT, 1978, Appl. Opt. **17**, 3034.
SMYTHE, R., and R. MOORE, 1984, Opt. Eng. **23**, 361.
SOMMARGREN, G.E., 1975, J. Opt. Soc. Am. **65**, 960.
SOMMARGREN, G.E., 1977, Appl. Opt. **16**, 1736.
SOMMARGREN, G.E., 1981, Appl. Opt. **20**, 610.
STETSON, K.A., and W.R. BROHINSKY, 1985, Appl. Opt. **24**, 3631.
TAKEDA, M., H. INA and S. KOBAYASHI, 1982, J. Opt. Soc. Am. **72**, 156.
THALMANN, R., and R. DÄNDLIKER, 1984, Proc. SPIE **492**, 299.
THALMANN, R., and R. DÄNDLIKER, 1985a, Opt. Eng. **24**, 930.
THALMANN, R., and R. DÄNDLIKER, 1985b, Proc. SPIE **599**, 141.
WILLEMIN, J.-F., and R. DÄNDLIKER, 1983, Opt. Lett. **8**, 102.

WOMACK, K.H., 1984a, Opt. Eng. **23**, 391.
WOMACK, K.H., 1984b, Opt. Eng. **23**, 396.
WYANT, J.C., 1975, Appl. Opt. **14**, 2622.
WYANT, J.C., 1982, Laser Focus (May), p. 65.
WYANT, J.C., 1985, Acta Polytech. Scand. Phys. **150**, 241.
WYANT, J.C., and K. CREATH, 1985, Laser Focus (November), p. 118.
WYANT, J.C., and R.N. SHAGAM, 1978, Use of electronic phase measurement techniques in optical testing, in: Optica Hoy y Mañana, Proc. 11th Congr. of the International Commission for Optics, Madrid, 10–17 September 1978, eds J. Bescos, A. Hidalgo, L. Plaza and J. Santamaria (Sociedad Española de Optica, Madrid) p. 659.
WYANT, J.C., B.F. OREB and P. HARIHARAN, 1984, Appl. Opt. **23**, 4020.
WYANT, J.C., C.L. KOLIOPOULOS, B. BHUSHAN and O.E. GEORGE, 1984, ASLE Trans. **27**, 101.
WYANT, J.C., C.L. KOLIOPOULOS, B. BHUSHAN and D. BASILA, 1985, J. Tribology, Trans. ASME **108**, 1.
YATAGAI, T., 1984, Appl. Opt. **23**, 3676.
YATAGAI, T., and T. KANOU, 1983, Proc. SPIE **429**, 136.
YATAGAI, T., and T. KANOU, 1984, Opt. Eng. **23**, 357.
YATAGAI, T., M. IDESAWA, Y. YAMASHI and M. SUZUKI, 1982, Opt. Eng. **21**, 901.
ZAVISLAN, J.M., and J.M. EASTMAN, 1985, Proc. SPIE **525**, 169.

AUTHOR INDEX